ELSEVIER

Contents lists available at ScienceDirect

Icarus

journal homepage: www.elsevier.com/locate/icarus



Research Paper

The effect of clay minerals on Li in martian groundwater simulant

Rachel Y. Sheppard ^{a,b,*}, Jessica M. Weber ^c, Laura E. Rodriguez ^d, Cathy Trejo ^c, Elisabeth M. Hausrath ^e, Laura M. Barge ^c

- a Planetary Science Institute, Tucson, AZ, USA
- ^b Institut d'Astrophysique Spatiale, Université Paris-Saclay, CNRS, Orsay, France
- ^c NASA Jet Propulsion Laboratory, California Institute of Technology, Pasadena, CA, USA
- d Lunar and Planetary Institute/USRA, Houston, TX, USA
- ^e University of Nevada Las Vegas, Las Vegas, NV, USA

ARTICLE INFO

Keywords:
Clay mineralogy
Groundwater
Li
Gale crater
Continuous flow reactor

ABSTRACT

The high mobility of Li allows it to be used as a tracer for groundwater processes, recording past aqueous conditions. On Earth, a relationship has been noted in multiple field sites between clay mineral abundances and elevated Li in bedrock. Observations from the Curiosity MSL mission at Gale crater on Mars showed a high-clay mineral and high-Li area near the Vera Rubin ridge (VRR) and Glen Torridon region, suggesting Li was perhaps substituting into clay minerals as was seen in these terrestrial field settings. However, the process of this substitution has not been examined in the laboratory using non-field samples, especially not with Mars-relevant mineralogy. To investigate this open question in the laboratory using Mars-relevant regolith and clay minerals, we conducted continuous flow packed-bed reactor experiments to test whether clay minerals affect the Li concentration of Mars regolith simulant MGS-1 during aqueous alteration. The mechanism for Li sorption was also investigated by conducting experiments with clays mixed with glass beads and investigating changes in other elements alongside Li via laser-induced breakdown spectroscopy (LIBS). We tested four dioctahedral clay minerals (kaolinite, illite, nontronite, mixed layer illite/smectite) and two trioctahedral clay minerals (talc, saponite) and found that both talc and illite are capable of increasing the amount of Li sorbed compared to MGS-1 simulant when exposed to Li-bearing groundwater. For MGS-1, the glass beads, and the clay minerals (talc, illite) the primary mechanism appears to be Li substitution for Mg, Al, and K, respectively. This has implications for ongoing Mars missions as well as astrobiology, specifically relating to understanding habitability of areas on Mars and identifying aqueous environments for future mission concepts.

1. Introduction

Li has been observed in nearly all classes of clay minerals on Earth, including sepiolite, illite, and smectites including montmorillonite and hectorite (Horstmann, 1957; Ashry, 1973). Weathering processes tend to remove highly soluble Li from minerals; this Li can then either be carried away by groundwater or incorporated into secondary products including clay minerals (Zawidzki, 1976; Starkey, 1982). This incorporation into clay minerals can occur via different mechanisms (Fig. 1) including adsorption onto the mineral surface, absorption into the bulk solid, and exchange for another ion at the solid surface, all of which mechanisms can be referred to as sorption (Horstmann, 1957; Ashry, 1973; Villumsen and Nielsen, 1976; Sposito, 1984; Williams and Hervig, 2005; Ajouyed et al., 2011). The ionic radius of Li makes substitution for Mg or K

relatively easy, which facilitates its incorporation into various clay minerals (Vine, 1980; Dehouck et al., 2022). This means that in terrestrial sediments Li is commonly elevated in the clay-size fraction (Starkey, 1982; Villumsen and Nielsen, 1976).

Starkey (1982) observed that natural trioctahedral smectites on Earth contain higher Li levels than dioctahedral smectites, although both types commonly contain Li. This indicates that the structural characteristics of clays influence Li incorporation. Furthermore, the variation of Li is related to grain size, indicating that finer grains, which have a higher surface area, can trap more Li (Villumsen and Nielsen, 1976). The adsorption capacity of clays increases significantly as grain size decreases, as smaller particles provide more active sites for ion exchange and Li retention. In particular, clay fractions smaller than 2 μ m, which are dominant in weathered and sedimentary environments,

^{*} Corresponding author at: Planetary Science Institute, Tucson, AZ, USA. *E-mail address:* rsheppard@psi.edu (R.Y. Sheppard).

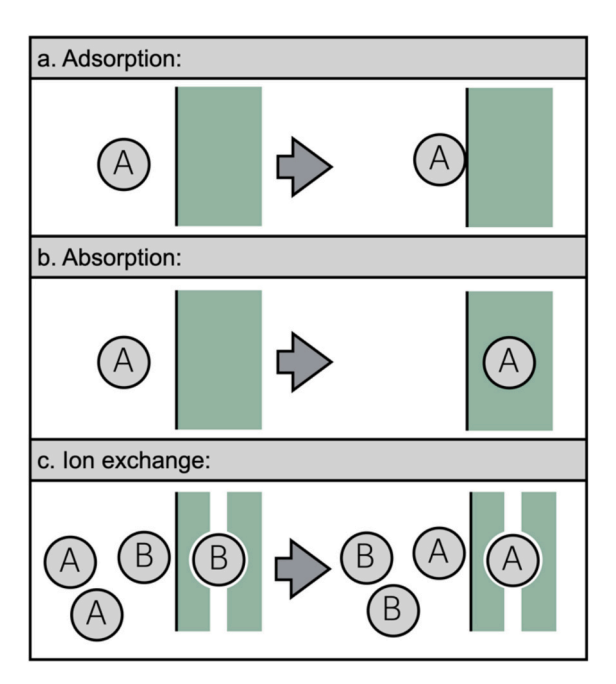


Fig. 1. Schematic showing (a.) adsorption to a clay mineral surface, (b.) absorption into a clay mineral bulk solid, and (c.) the reversible process of ion exchange.

exhibit enhanced Li uptake due to their high cation exchange capacity and increased reactivity. This variation also seems to be related to the content of montmorillonite in the clay fraction, highlighting the importance of specific clay types in Li trapping. On a larger scale, this means Li can become concentrated in basins and lake sediments (Benson et al., 2017), where finer-grained clays accumulate due to their suspension in water and subsequent deposition in low-energy environments.

Gale crater, a ~ 155-km-wide impact basin on Mars, preserves evidence of an ancient lake system that persisted through multiple depositional episodes during the Hesperian period (Grotzinger et al., 2014). This long-lived lake is recorded in the finely laminated mudstones which were deposited in a predominantly lacustrine environment at the base of Mount Sharp. These mudstones are composed of fine-grained sediments (<64 µm grain size) exhibiting millimeter- to centimeter-scale laminations, consistent with deposition under quiescent conditions (Grotzinger et al., 2014; Grotzinger et al., 2015; Hurowitz et al., 2017). However, variations within the stratigraphy, including cross-bedded sandstones, scour-and-drape structures, and thin coarser-grained beds, suggest episodic reworking of sediments by fluvial and deltaic processes (Grotzinger et al., 2014; Edgar et al., 2017). The Yellowknife Bay formation, for example, records the progradation of a sandy fluvial system into a shallow lake, providing the first evidence of a habitable environment explored by the Curiosity rover (Grotzinger et al., 2014).

As Curiosity ascended Mount Sharp, evidence for sustained lacustrine conditions continued through Vera Rubin ridge and the clay mineral rich Glen Torridon region. Vera Rubin ridge, a topographic high within the Murray formation, preserves laminated mudstones indicative of lakebed deposition, though diagenetic alteration, including hematite enrichment and cementation, suggests later groundwater interactions that modified its mineralogy (Bristow et al., 2018a, 2018b; Frydenvang et al., 2020). Glen Torridon, stratigraphically above VRR, is rich in phyllosilicates, particularly smectite clays, suggesting prolonged aqueous alteration and a continuation of lake conditions (Rampe et al., 2020a, 2020b; Sheppard et al., 2020; Rudolph et al., 2022; Fedo et al., 2022). While lacustrine deposition dominated both regions, localized sedimentary structures suggest intermittent fluvial or deltaic influence (Fedo et al., 2022).

Observations from Curiosity's ChemCam laser-induced breakdown spectroscopy (LIBS) instrument showed elevated levels of Li in regions rich in clay minerals. The Li spike was attributed to Li specifically hosted in clay minerals; consequently, Li was proposed as a potential proxy for clay mineral abundance in some areas of Gale crater (Frydenvang et al., 2020; Bristow et al., 2021; Dehouck et al., 2022). If so, then this would be valuable since elemental abundance data (via ChemCam's Laser Induced Breakdown Spectroscopy (LIBS) instrument) is collected more regularly than mineralogical data (via the CheMin X-ray diffractometer, XRD).

Gale crater rocks generally contain 5–10 ppm Li, sometimes as high as 80 ppm (Fairén et al., 2015). As the rover traversed across the Vera Rubin ridge multiple times, a trend emerged. Both Li and the chemical index of alteration (CIA) were not seen to follow elevation but rather morphology, and both were elevated before and after the VRR, in areas measured separately by CheMin to be higher in clay minerals (Fig. 2; Bristow et al., 2015, 2018a, b; Frydenvang et al., 2020; Rampe et al., 2020a, 2020b).

The presence of clay minerals in Gale crater implies past aqueous activity, which could have facilitated the dissolution, movement, and eventual trapping of Li in a manner similar to that observed on Earth. As the clay minerals in Mt. Sharp, a central peak within Gale crater, are a mix of detrital and authigenic origins (Vaniman et al., 2014; Bristow et al., 2015, 2018a, b; Thorpe et al., 2022), initial clay mineral deposition could have subsequent effects on later diagenetic fluid events. This dynamic interaction suggests that Li content in these minerals could provide insights into the ancient Martian environment, including changes in pH, temperature, and the availability of water. However, this has not been tested in the laboratory with Mars-relevant mineralogy.

In this work we conducted continuous flow experiments designed to test Li mobility through columns of porous media doped with clays. The porous media was either a Mars simulant or an inert matrix (glass beads); and the clays were selected to represent different types of relevant clays on Mars, as described below. Li-bearing water (to simulate groundwater enriched in Li leached from bedrock) was flowed through the column, and the contents of the porous matrix and clays were analyzed for concentration of Li to determine its mobility in these simulated geochemical environments. This work can improve our understanding of Mars aqueous processes, including subsurface water-rock interactions.

2. Methods

2.1. Mineral simulant selection and prep

2.1.1. Packed-bed matrix

MGS-1: MGS-1 is a Mars regolith simulant prepared by the CLASS Exolith Lab at UCF that is commercially available as a mineralogical and chemical simulant of the Mars regolith. Its composition is based on the Rocknest soil observed by the *Curiosity* rover in Gale crater (Cannon et al., 2019). This portion was purchased in 2021. Prior to beginning experiments, the chemistry, mineralogy, and particle size of this particular MGS-1 portion was analyzed by Clark Testing using ICP-OES and X-ray diffractometry, respectively (Table 1).

The MGS-1 simulant does not contain appreciable Li (Table 1) which is to be expected since Li is more likely to remain in solution than to be incorporated in mineral phases (Wimpenny et al., 2010). Therefore, for these experiments we chose to include Li in the simulated groundwater fluid in order to observe its incorporation into clays within the column (Section 2.1.3). The MGS-1 was used as received and was not otherwise heated or rinsed before experiments.

Glass beads: The 3 mm glass beads (Cole Parmer) were used as received and were not otherwise heated or rinsed before experiments.

2.1.2. Clay minerals

We tested 4 dioctahedral clay minerals (kaolinite, illite, nontronite,

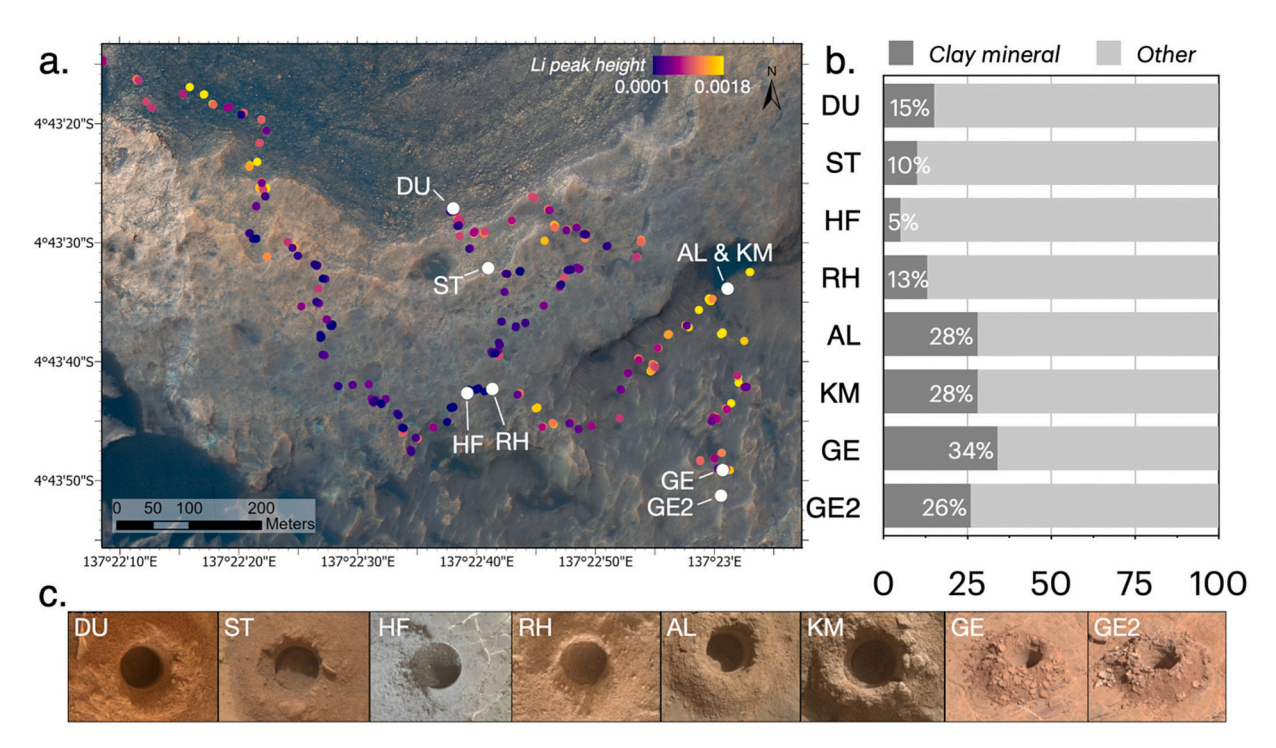


Fig. 2. (a.) HiRISE imagery of Vera Rubin ridge, with Li peak height in ChemCam LIBS data in colored dots. CheMin drill holes are marked with white dots: Duluth (DU, sol 2057), Stoer (ST, sol 2136), Highfield (HF, sol 2224), Rock Hall (RH, sol 2261), Aberlady (AL, sol 2369), Kilmarie (KM, sol 2384), Glen Etive (GE, sol 2486), and Glen Etive 2 (GE2, sol 2527). (b.) CheMin normalized results in wt% of the drill holes divided into clay minerals (dark gray) vs. other crystalline phases (light gray). AL & KM peaks are at 9.2 Å and have been modeled as talc (Bristow et al., 2021; Tu et al., 2021; Thorpe et al., 2022). (c.) Images of each relevant drill hole.

Table 1

Elemental abundance (ICP) and XRD results of the MGS-1 Mars regolith simulant. Oxide concentrations were calculated from elemental wt% and normalized to 100 wt % across the measured oxides to facilitate compositional comparison. XRD key: feldspar (fel.), olivine (ol), pyroxene (pyx), gypsum (gy.), ferrihydrite (fer.), magnetite (mag.), quartz (qz.). All value are in wt%.

ICP	Al ₂ O ₃	<i>CaO</i>	Cr ₂ O ₃	FeO	K ₂ O	<i>MgO</i>	MnO	Na ₂ O	P ₂ O ₅	SiO ₂	TiO ₂
	14.88	8.99	0.24	11.81	0.49	15.71	0.12	1.79	0.35	45.25	0.39
XRD	Fel. 68.6		Ol. 6.1	Pyx. 7.6		Gy. 6.1		Fer. Mag. 5.2 4.3		-	Qz. 2.2

mixed layer illite/smectite) and 2 trioctahedral clay minerals (talc, saponite). Mineralogy of the starting clays was validated using reflectance spectroscopy (Fig. 3).

The kaolinite used was Clay Minerals Society KGa-1b which is low-defect kaolinite from Georgia, USA. The illite used was IMt-2 from Montana, USA. The nontronite used was Clay Minerals Society Nau-2. The mixed-layer illite-smectite (I/S) used was Clay Minerals Society ISCz-1. The talc used was laboratory-grade from Aldon talc sieved to 325 mesh. The saponite was synthesized in the laboratory based on previous work synthesizing the ferric smectite nontronite (Decarreau et al., 2008; Mizutani et al., 1991; Gainey et al., 2017), which is formed from a ferrous precursor, and ferrous saponites (Baldermann et al., 2018; Chemtob et al., 2015; Sakuma et al., 2022). Therefore, to synthesize the ferrous saponite, instead of the ferrous precursor being oxidized, it was dried in an anaerobic chamber; digestion followed by measurement of the ferrozine method showed >80 % ferrous Fe, and glycolation shows expansion characteristic of smectites such as saponites.

The synthetic clay minerals may be more poorly crystalline than the natural standards due to synthesis over laboratory time scales rather than natural field time scales. However, clay minerals in natural environments may also be less crystalline than the Clay Minerals Society natural standards.

All clay minerals were ground to ${\sim}1\text{--}5~\mu m$ particle size using an

agate mortar and pestle.

2.1.3. Groundwater simulant

For pure water experiments, Milli-Q water (18.2 M Ω •cm) was used. For Li-bearing groundwater simulant, 100 mM LiCl concentration groundwater was prepared by combining 500 mL Milli-Q water with 2.1195 g LiCl. Modeling of the Gale crater groundwater by Schwenzer et al. (2016) suggest a total dissolved solids concentration of 1.8–4.7 · 10^{-2} mol/L, which is equivalent to 18–47 mM. We opted for a concentration approximately $2\times$ higher than this upper modeled range due to the restricted time available in laboratory experiments. We believe this concentration is still geologically meaningful as a review of terrestrial reservoirs shows Li concentrations spanning \sim 6–226 mM (Dugamin et al., 2021). Nevertheless, as we studied the degree to which Li is sorbed to different martian analog samples, our results remain geologically meaningful and representative of real changes that may have occurred in the martian groundwater system.

2.2. Experimental methodology

Experiments were carried out in two batches with and without a capping clay-enriched layer: MGS-1 simulant experiments (Experiments 1–14, Section 2.2.2) simulated the Mars regolith under Li-bearing fluid

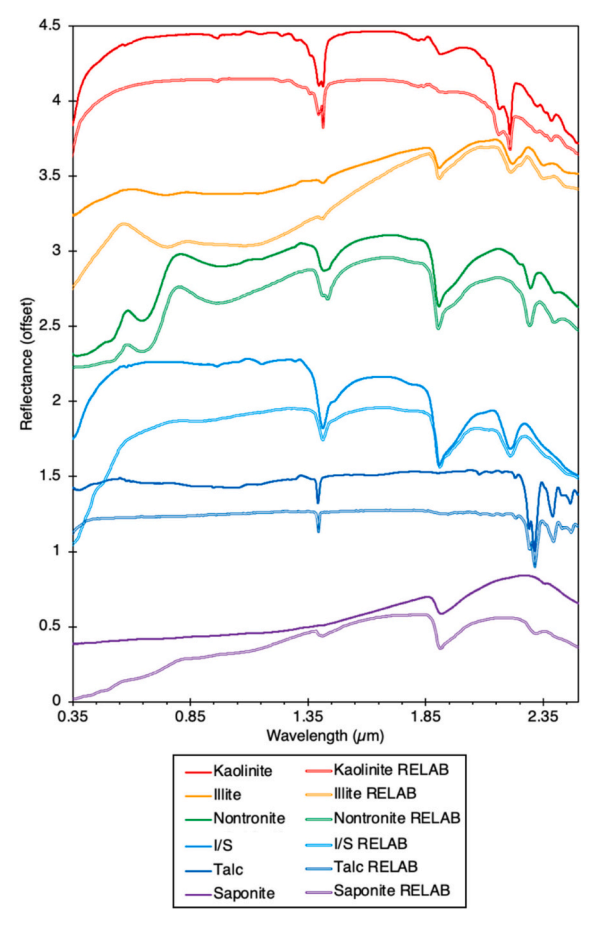


Fig. 3. Laboratory reflectance spectra of the clay samples used in this study (solid lines) and RELAB spectra for comparison (double lines below each natural sample). Pairs from top to bottom are: kaolinite (red), illite (orange), nontronite (green), mixed-layer illite/smectite (light blue), talc (dark blue), and saponite (purple). RELAB sample name and mineral information: kaolinite (JB-JLB-766, KGa-1b), illite (JB-JLB-782, CMS Standard IMt-1), nontronite (BE-JFM-015, Nau-2), mixed-layer illite/smectite (JB-JLB-261, IsMt-2), talc (EC-EAC-006, PIG006), saponite (SA-EAC-059, SAP103). (For interpretation of the references to colour in this figure legend, the reader is referred to the web version of this article.)

system conditions; and glass bead experiments (Experiments 15–28, Section 2.2.3) served as controls to deduce the effects of Li-bearing fluids on the capping clay minerals. Both sets of experiments utilized the same clay minerals to cap the MGS-1 or glass packed columns as described in Section 2.1.3.

2.2.1. Packed-bed reactor setup

All experiments utilized the continuous flow or flow-through reactor setup shown in Fig. 4, where two 250 mm Diba Omnifit® EZ chromatography columns utilized as packed beds were chained together with 0.03-in. i.d. tubing (e.g., Weber et al., 2024). A Harvard auto-syringe pushed 30 mL of the relevant fluid through the column at 0.2 mL/min. All water outflow from the column was collected in a 50 mL Falcon tube and frozen. Liquid analysis was not carried out as it was outside the scope of this project.

Using two packed-beds allows for separate analysis of the clay-bearing vs. non-clay-bearing regolith simulants. We use this reactor setup to test the hypothesis that if a clay mineral is capable of increasing in Li content due to exposure to Li-bearing fluids, packed bed A will show no change in Li content and clay-bearing packed bed B will show an increase in Li.

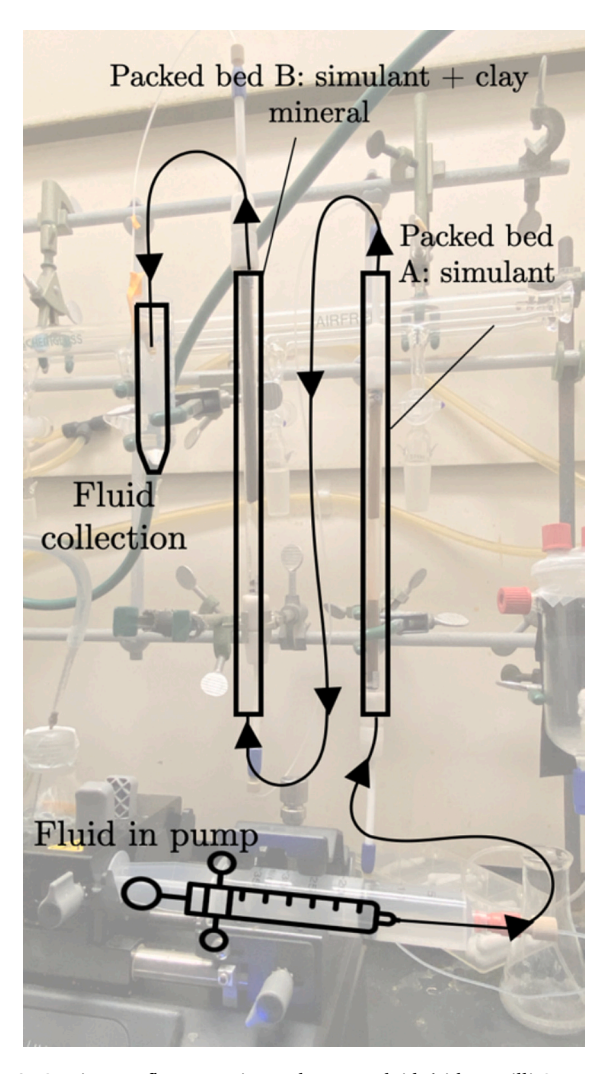


Fig. 4. Continuous flow experimental setup. Fluid (either Milli-Q water or water +100 mM LiCl) was pushed via automatic syringe through packed bed A (MGS-1 or glass beads only), packed bed B (MGS-1 or glass beads + clay mineral) and finally into a Falcon tube for fluid collection.

2.2.2. Simulant experiments

The MGS-1 experiments (Experiments 1–14) are summarized in Fig. 5. The packed beds could contain about 8 g of dry sediment; to account for any swelling once water was percolated through, we limited the volume of material to 7.5 g to avoid clogging the system. Packed bed A contained 7.5 g MGS-1. For control experiments (Experiments 1 and 2), packed bed B also contained only 7.5 g MGS-1 and no clay. For clay mineral experiments, packed bed B contained 6 g MGS-1 + 1.5 g of the relevant clay mineral; this means the clay constituted 20 wt% of the mixture, which is appropriate for Glen Torridon clay mineral abundance (Fig. 2; Sheppard et al., 2021; Thorpe et al., 2022; Morrison et al., 2024). Clays and MGS-1 were physically mixed in a sealed Falcon tube before adding to the packed bed.

2.2.3. Glass bead experiments

The glass bead experiments (Experiments 15–28) are summarized in Fig. 6. Packed bed A contained 7.5 g glass beads. For control experiments (Experiments 15 and 16), packed bed B also contained only 7.5 g glass beads. For clay mineral experiments, packed bed B contained 6 g glass beads ± 1.5 g relevant clay mineral, physically mixed before adding to the packed bed.

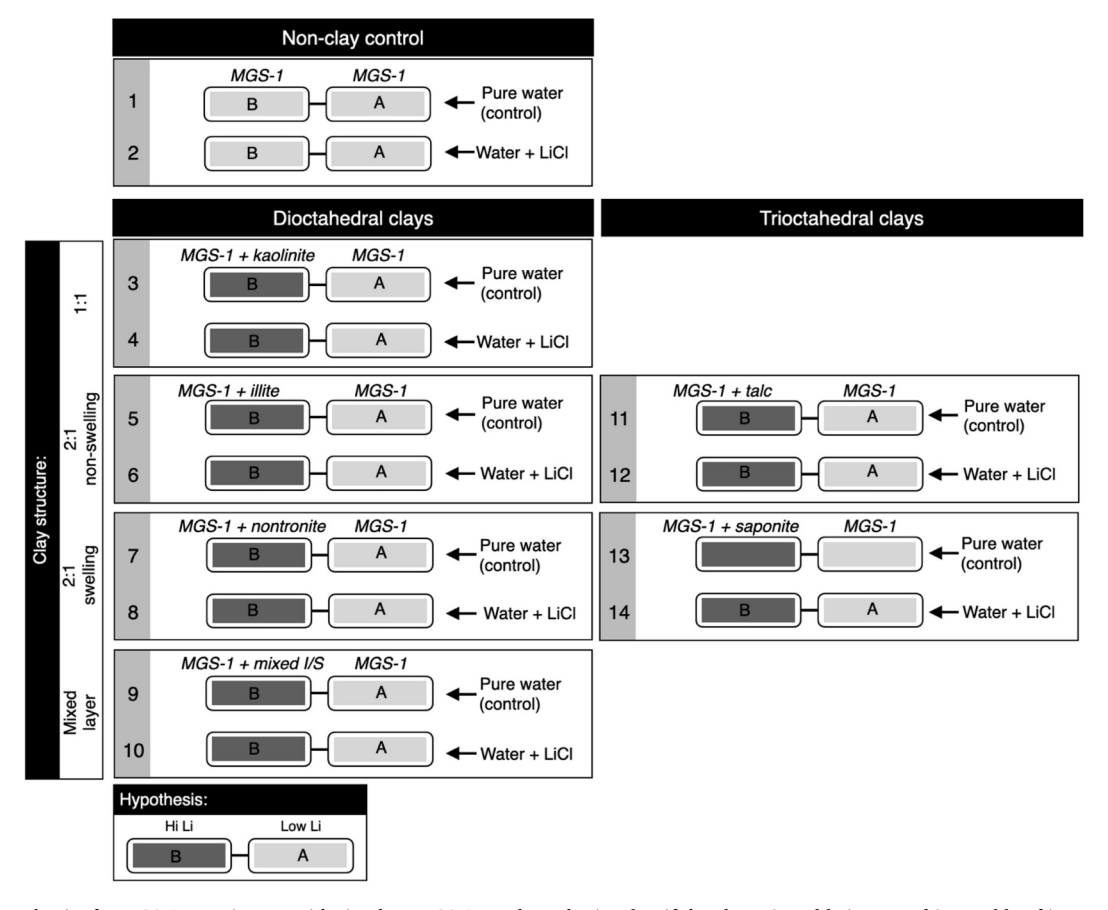


Fig. 5. Experimental suite for MGS-1 experiments with simulant MGS-1. We hypothesize that if the clay mineral being tested is capable of increasing in Li content due to exposure to Li-bearing fluids, packed bed A will show no change in Li content and clay-bearing packed bed B (dark gray) will show an increase in Li. (Note: I/S is mixed-layer illite/smectite.)

2.2.4. Post-experimental handling

Upon completion of the experiment, the material in packed beds A and B was collected in separate labelled Falcon tubes frozen and then freeze-dried overnight in an AdVantage freeze dryer. VNIR spectra were collected of the dried material. Spectra were collected of the dried mixtures and then the mixtures were powdered using a rock crusher to homogenize the material for LIBS.

2.3. Reflectance spectra

Reflectance spectra of the freeze-dried sample were collected using an Analytical Spectral Devices (ASD) FieldSpecPro spectroradiometer which collected reflectance spectra data from 0.35 to 2.5 μ m. Spectra were collected based on a Spectralon white reference and using the ASD contact probe. Simulant was placed on Cinefoil, a highly absorbing matte black surface.

2.4. Laser-induced breakdown spectroscopy (LIBS)

Dried samples were powdered using an agate stone mortar and pestle for 5–10 min. Samples were then made into 13 mm diameter pellets by applying 8 tons of force for 10 min using a manually operated benchtop 12-ton SpectroPress (4312, Chemplex Industries, Inc.). Pellets were analyzed using a custom lab grade LIBS Chemical Imaging system built by Impossible Sensing (1060 nm Red Energy Fiber laser, 20 W at 33 kHz). Settings were optimized for the analysis of these particular samples (250 shots, pulse repetition frequency: 20,000 Hz). Each sample was analyzed at 10–20 different locations to minimize variation due to sample heterogeneity.

2.4.1. LIBS processing

The LIBS instrument is composed of three spectrometers that collect from the near-UV, visible, and near-infrared regions. All data were processed using R software. As each region has a different signal-to-noise ratio and background, each of the three regions were pre-processed separately before being combined to generate a single spectrum. Pre-processing involved trimming the overlapping ends of each spectrum, denoising using the wavshrink function in the wtmsa package (Constantine and Percival, 2017) and correcting for the Bremsstrahlung effect on the baseline using the rollingBall method in the baseline package (Liland et al., 2010). The three regions were then combined to form a single spectrum. To correct for intensity changes due to inherent shot-to-shot variations and matrix effects, each spectrum was normalized to the sum intensity over the entire spectrum.

2.4.2. Calculating peak areas

Peaks were deconvolved using the Levenberg-Marquardt optimizer (nlsLM function in the minpack.lm package; (Elzhov et al., 2023)) to fit a Pseudo-Voigt function to a narrow (\sim 2–6 nm) spectral window centered at a pre-selected peak of interest (Thomas et al., 2018). This process searches for fits to several parameters in the Pseudo-Voigt equation that optimizes the fit with the raw data. The parameters describe each peak and include: the peak center (nm), intensity, full-width half max, and the proportion of Gaussian to Lorentzian. The number of peaks as well as a starting guess and constraints for each parameter were derived in R for each spectral window, leveraging first and second derivatives of the narrow spectrum of interest. Fits that had a root mean square error > 0.1 were considered a poor fit and not used in subsequent analyses. The deconvolved peaks were integrated to calculate area (see Fig. 7 for an example LIBS spectrum and Fig. 8 for examples of the deconvolved peak

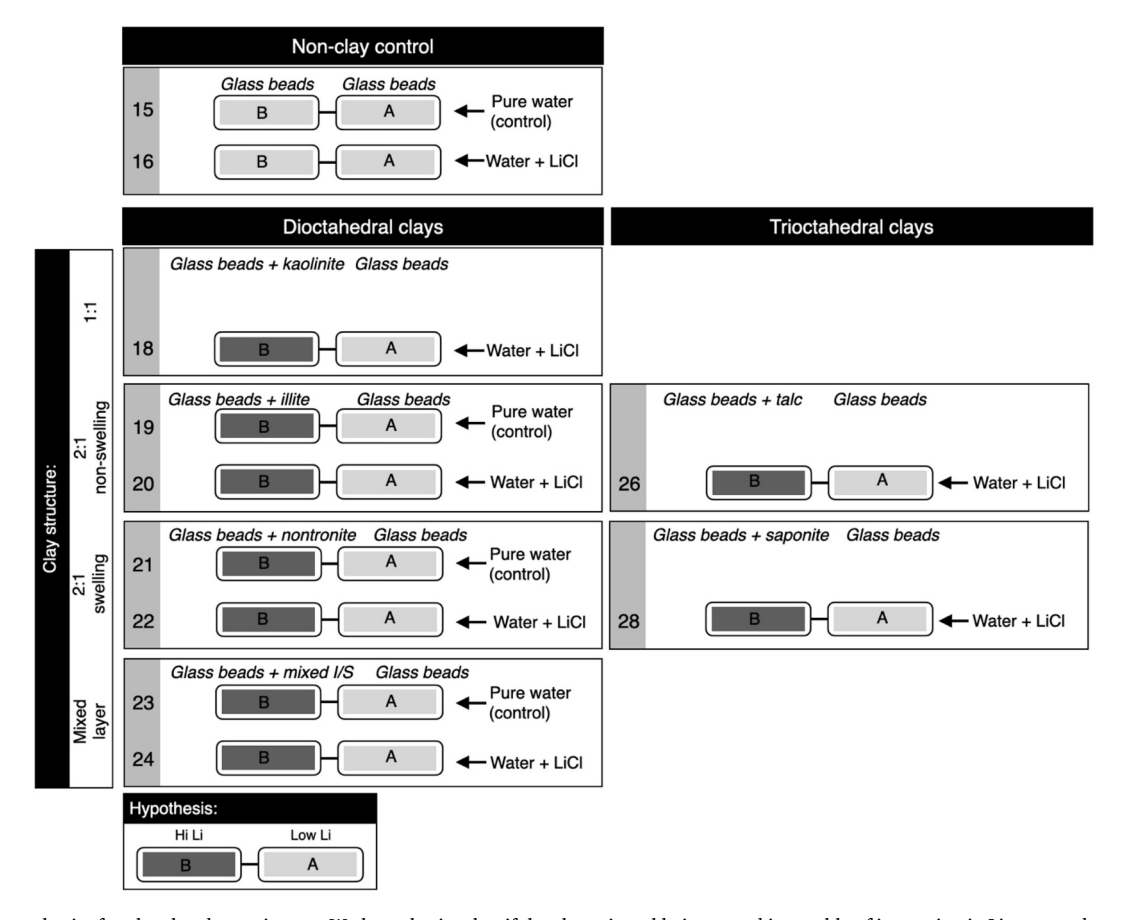


Fig. 6. Experimental suite for glass bead experiments. We hypothesize that if the clay mineral being tested is capable of increasing in Li content due to exposure to Libearing fluids, packed bed A will show no change in Li content and clay-bearing packed bed B (dark gray) will show an increase in Li. (Note: I/S is mixed-layer illite/smectite.)

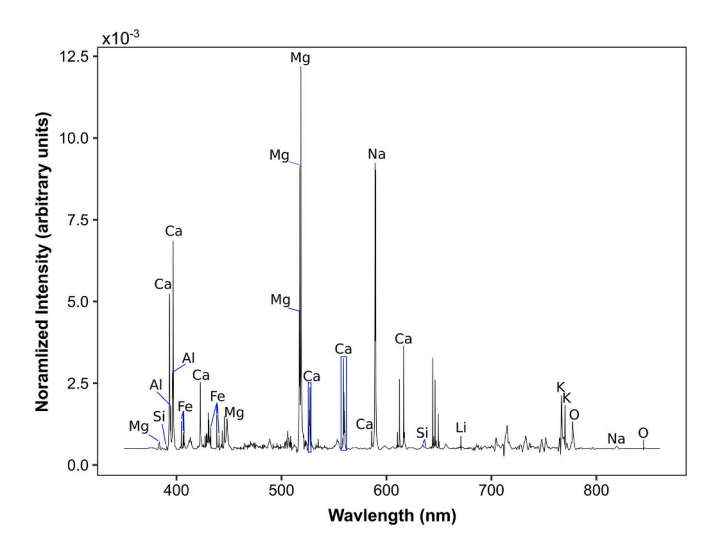


Fig. 7. Example of a typical LIBS spectrum that was analyzed. Shown is the average spectrum of the MGS-1 dry control whose peaks have been annotated with the elements of interest for this work. Note that Li (670.8 nm) was observed in the sample, suggesting that the martian simulant has some Li prior to being exposed to any fluids. The blue lines indicate which emission line belongs to the labelled element. Boxed lines indicate multiple emission lines that belong to the labelled element. (For interpretation of the references to colour in this figure legend, the reader is referred to the web version of this article.)

fits). The process by which Li was sorbed or precipitated onto the sample was also tested by determining whether there were any significant changes in the abundance of other prominent cations present within the sample upon exposure to the LiCl solution. The emission lines selected for peak deconvolution were as follows: Li: 670.8 nm, Al: 394.4 nm, Fe: 432.6 nm, Na: 589.2 nm, Ca: 393.5 nm, K: 766.7 nm, Mg: 518.5 nm, and Si: 390.6 nm.

To determine the accuracy of using peak areas of the selected emission lines to evaluate changes in elemental abundances with exposure to the LiCl solution, we first compared the raw peak areas of the glass beads with the MGS-1 simulant (Fig. 10). We also investigated whether changes in peak areas would accurately reflect the elemental composition of the added clays (Fig. S3, S4). To determine how adding clays to the experimental set up impacted the elemental peak areas in samples exposed to water or LiCl we subtracted the median of the respective control (i.e., column A or B of the glass beads or MGS-1 based samples exposed to water or LiCl; Fig. 9) from the peak areas derived from the corresponding experimental samples (results shown in Figs. 10–12; Figs. S4, S6). The median was selected to correct for background elemental abundances instead of the mean because the peak areas were consistently not normally distributed and included outliers.

2.4.3. Statistical analyses

For each sample, areas that fell outside $1.5\times$ the inner quartile range were considered outliers and removed. Given the non-normal distribution of some of the elemental data we conducted a Kruskal-Wallis test followed by pairwise Wilcox tests to determine if there were significant differences in the area of the elemental peaks within different matrices (glass beads, MGS1 simulant, and a mixture of MGS-1 with kaolinite, illite, talc, saponite, nontronite, and an illite/smectite mixture) before

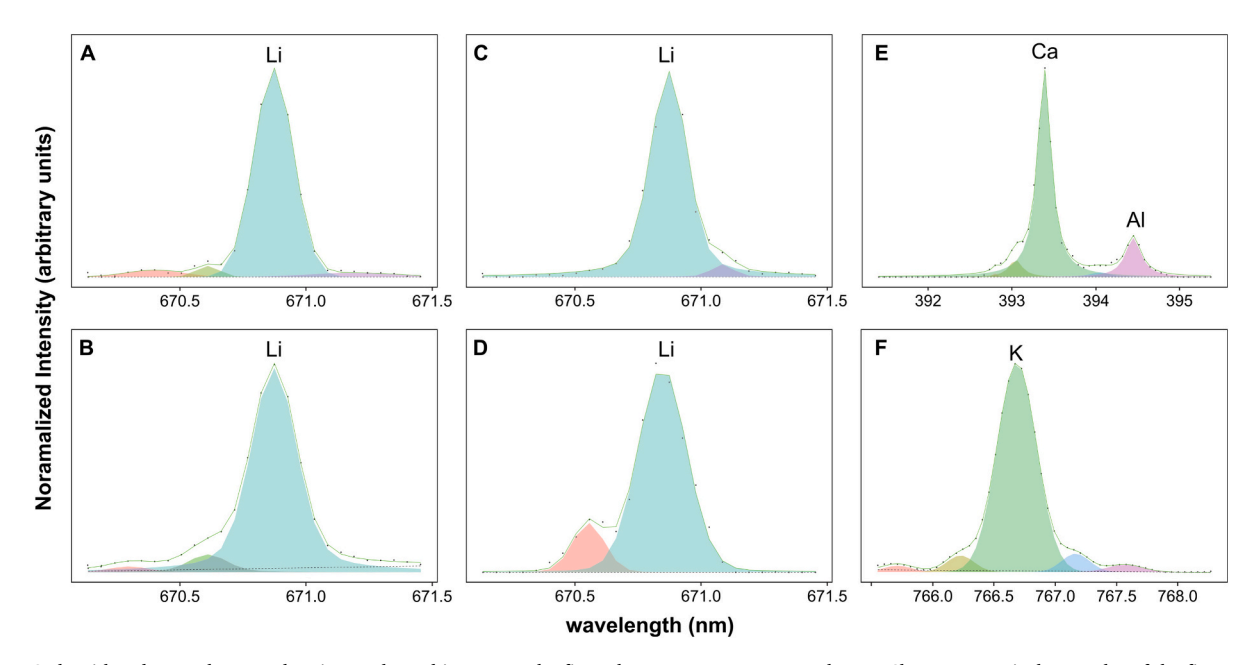


Fig. 8. LIBS algorithm deconvolves overlapping peaks and integrates the fit peaks to get an accurate peak area. Shown are typical examples of the fits. Dots are the raw data points, green line is the overall fit, the shaded regions are the deconvolved peaks, and the dashed line is the linear fit of the background continuum. (A-D) Peak fits in the Li region for four samples (A – Glass beads, Column A exposed to LiCl solution; B – Glass beads packed with saponite clay (Column B) exposed to LiCl solution; C – Glass beads, Column A exposed to LiCl solution (different point than A); E – MGS-1 packed with talc (Column B) exposed to water (no LiCl)). E – highlights the region used to acquire peak areas for Ca and Al (sample shown: MGS-1 dry standard). F – an example of the fit for deconvolving the K peak (sample shown: Glass beads not packed with any clays (Column B) exposed to water (no LiCl)). (For interpretation of the references to colour in this figure legend, the reader is referred to the web version of this article.)

and after being subjected to a flowing solution of pure water or 100 mM LiCl).

3. Results

3.1. LIBS

Note that the LIBS spectra and deconvolved areas corresponding to Li, Fe, Mg, Si, Al, Ca, Na, and K are provided as supplementary files (see data availability statement).

3.1.1. Experimental controls

We used LIBS to measure Li and other cations in the glass beads and MGS-1 pellets. A small Li peak (670.8 nm) was seen even in a control sample of MGS-1 that was not used in a continuous flow experiment. Using elemental standards (Fe, Mg, Si, Al, Ti, C) and the NIST LIBS database we confirmed that prominent elements did not interfere with the Li peak. Li was not reported in the MGS-1 simulant by Cannon et al. (2019) (Table 1), however elemental abundances were determined by XRF, which cannot detect Li. The presence of a Li peak in a control sample for MGS-1 (Fig. 7) suggests that the Li is not a result of contamination from the experimental set up or water, but rather Li that is inherently present in the sample.

As expected, the glass beads contained more Si and significantly less Al, Fe, Na, K, and Mg than MGS-1. Surprisingly, LIBS showed that the glass beads contained significantly more Li than the isolated MGS-1 simulant. The difference in Li between the A (non-clay-bearing) and B columns (clay bearing, except for these controls which contained more of the same matrix) for both controls was negligible (Fig. 9; p=0.39 for MGS-1 and p=0.98 for glass beads). In fact, no significant changes were observed for any of the elements between columns A and B for either the glass or MGS-1 samples apart from K (p=0.03) for MGS-1 and Ca (p=0.008) as well as Si for glass (p=0.02). Thus, any difference in the elemental abundances (except K for MGS-1 and Ca/Si for glass) seen between the A and B columns can be attributed to the particular clay

added to column B.

Importantly, differences in elemental abundances between the glass bead and MGS-1 experiments could be partially due to matrix effects which stem from differences in the efficiency with which the laser coupled with the sample matrix. For samples that couple better (typically those with more Fe and are darker colored), the LIBS signal will have a good signal-to-noise ratio; laser coupling and the resulting plasma temperature will also impact the ionization of elements and their relative ratios. Consequently, it is best to keep comparisons of elemental abundances reserved to samples with the same or similar matrices. For this reason, we treat changes in elemental abundances between the two experimental set ups (glass beads or MGS-1) separately. We also investigated the validity of comparing the effects of different clays on different elements for each mineral matrix (e.g., Fig. S3 and S4 discussed more in the subsequent paragraphs). Finally, to further mitigate matrix effects on raw intensities, all spectra were normalized as described in the methods. Note that LIBS is an inherently semi-quantitative technique, producing elemental intensities that often require multivariate calibrations (produced from the same matrix) to acquire quantitative values. As our main question stemmed from whether clays could enhance Li sorption to a degree that was observable by LIBS (rather than deducing exactly how much was sorbed), we report changes in elemental abundances in arbitrary units (derived from integrated peak areas) rather than quantitative abundances.

Fig. 10 shows the relative differences in the Li peak area after passing pure water through experiments containing clay in column B relative to the control experiments that lacked clays (Fig. 9). Note that with the two exceptions of the MGS-1 experiment with kaolinite and the glass beads experiment with nontronite, there was no significant change (as expected) between columns B and A. This confirms that any changes observed after passing a Li solution through the system (Fig. 11) reflect increased/decreased Li sorption resulting from the addition of a particular clay. Kaolinite and nontronite, having more Li in column B vs column A suggests that there is more preexisting Li present within the two clays than the MGS-1 simulant and glass beads, respectively. The

Glass & MGS-1 samples exposed to water

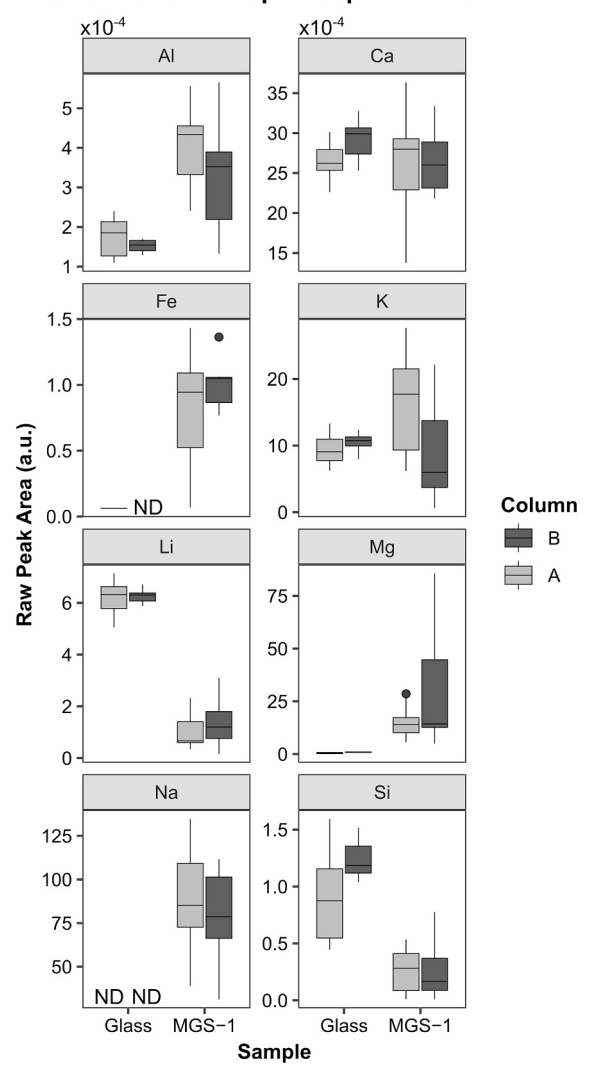


Fig. 9. Control results for the continuous flow setup. Plotted are the raw peak areas of various cations including Li observed by LIBS analysis of two connected packed beds A & B (top panel of Figs. 4–5). The median of these two experiments is used to correct for preexisting Li present in the glass beads or MGS-1 simulant so that any changes in the Li or other elemental signals due to the replacement of 50 % of the glass/MGS-1 matrix with clays (Fig. 10) could be determined. Note that the glass beads had significantly more Li than the MGS-1 sample. For Li, the differences between the A and B columns for both experiments were determined to be not statistically significant (p = 0.39 for MGS-1 and p = 0.98 for glass experiments). ND = not detected. a.u. = arbitrary units.

column A filled with glass beads in the nontronite experimental set also had more Li than the corresponding control column A (Fig. 10), even though no clay was present in this column; this suggests that the sample started off with more Li than the control experiment, possibly due to contamination within the glass beads used in that set up. Accordingly, the Li content of column B of that set (glass beads + nontronite) was also elevated more than all the other samples including MGS-1 with nontronite.

To deduce how Li could be sorbing or precipitating onto the sample we wanted to test how changes in Li corresponded to changes in other prominent cations. However, before this could be done, we needed to confirm whether the areas of the selected peaks accurately reflected changes in the elemental chemistry of the samples. To this end we plotted the elemental abundance of all the cations of interest from the control water experiments containing clays mixed with glass beads and

MGS-1 in Fig. S3 and Fig. S4, respectively. Table S1 summarizes the chemical formula and the elemental abundance for the source clays as reported by the vendor. Table 2 summarizes the chemical formula and predicted elemental composition for the column B experiments by combining 50 % of the elemental abundances from MGS-1 with 50 % of the elemental abundances of the source clays reported in Table S1 (simulating the mixing of MGS-1 and clay 1:1 in Column B).

3.1.2. Elemental variation in glass with clays

Based on Table 2 we would predict that kaolinite samples would have the strongest Al signal (followed by illite and illite/smectite), talc the most intense Mg signal (followed closely by MGS-1 control), illite the most intense K signal (followed by illite/smectite), MGS-1 the most intense Ca signal (followed by nontronite) and saponite the strongest Fe signal. Generally, we found that our LIBS observations were consistent with these predictions except for Ca and Na. We observed that talc had the highest levels of Mg (p < 0.05 amongst all experiments except MGS-1 where p = 0.23), illite and kaolinite had the most intense Al peaks, K was most intense (in decreasing order) within the illite, illite/smectite, and kaolinite experiments (though the difference amongst these three were not statistically significant), and nontronite had the most intense median value for Fe (though the difference amongst the other samples was not statistically significant). Overall, our data suggests that the Al, K, and Mg peaks may be informative for investigating the mechanism for Li sorption/precipitation in our subsequent experiments. These relative peak areas for these elements in the glass experiments containing clays also accurately reflected the distributions we would expect given the elemental composition of the source clays (see SI text and Fig. S3).

Our results for Fe, Na, Ca, and Si suggest that the relative abundance of these elements may not be accurately represented by their peak areas. Indeed, for our glass experiments we found that the low levels of Fe and Na were problematic for LIBS detection; changes in the Ca intensity amongst the glass experiments also did not correspond to predicted Ca abundances (see SI text and Fig. S3). For MGS-1, although nontronite had the largest median signal for Fe, it was not significantly different compared to the other experiments as it should have been given that samples containing it should have about twice the amount of Fe as the MGS-1 control and about $4\times$ the Fe content in samples mixed with kaolinite, talc, or illite/smectite (Table 2). While iron is known to generate a strong LIBS signal, the prominent iron peaks are typically in the UV region, below what was measured by the instrument. Indeed, the iron peak we selected (432.6 nm) is expected to be relatively weak compared to the UV peaks (NIST LIBS Database). We also observed that kaolinite was the most enriched in Na compared to the MGS-1 control (p < 0.02). Notably, the Na abundance did not vary significantly amongst the samples (Na₂O ranging from 0.9 to 1.8 wt%) - thus, it may be that the precision of the LIBS instrument is responsible for this discrepancy. For Ca we found that talc had the strongest signal (p < 0.01 between talc and all experiments except saponite where p = 0.13) rather than MGS-1 or nontronite as was expected; the abundance of CaO in experiments mixed with talc is ~4.4 wt%, with MGS-1 only ~8.9 wt%, and with nontronite is ~5.8 wt%. One possibility for this discrepancy could be due to saturation of the detector and self-shielding of the Ca line. Ca generates very strong emission lines and were occasionally found to have saturated the detector; we also observed splitting of the Ca peak. To combat this, we had summed up the area of the split peak and treated it as a single area for Ca, however this approach may have introduced error. Finally, we observed that the Si signal was highest in the illite experiment; although this difference is considered statistically significant compared to the other experiments, the difference may not be meaningful given the relatively weak Si signal (thus the differences are relatively minor compared to changes observed amongst the other elements).

3.1.3. Changes in Li sorption due to presence of clays

Flowing a solution of 100 mM LiCl through the system enabled us to

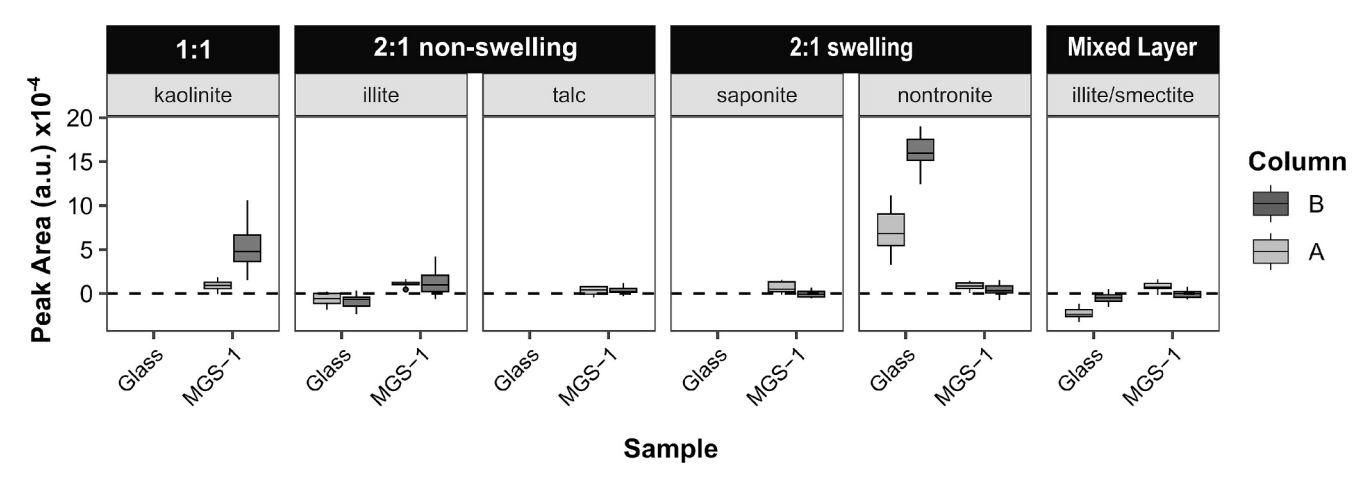


Fig. 10. Control results with clays. The difference in Li content observed by LIBS between mineral matrices exposed to a flowing solution of pure Milli-Q water and the corresponding glass or MGS-1 control column that was exposed to pure water with no additional clays (i.e. column A of the same experimental set up in Fig. 9). The dashed horizontal line represents the baseline from the corresponding control. Fig. S3 plots the difference in abundance between Column B (containing clays) and Column B of the control (no clays as shown in Fig. 9) for each cation of interest. a.u. = arbitrary units.

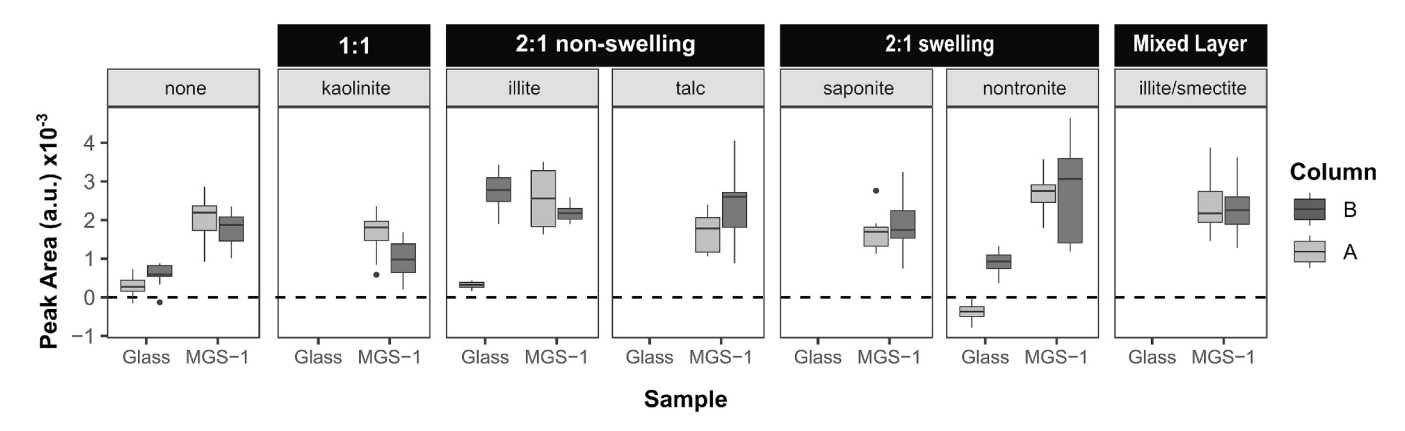


Fig. 11. Experimental results with LiCl solution. The difference in Li content observed by LIBS between mineral matrices exposed to a flowing solution of 100 mM Li and the corresponding control that was exposed to pure water (i.e. column A or B of the same experimental set up in Fig. 10). The difference was calculated to assess whether any changes in Li were due to the sorption capability of the clays themselves. The dashed horizontal line represents the baseline from the corresponding control. Note that the glass beads did not sorb nearly as much Li compared to all other mineral matrices, including the MGS-1 simulant without any additional clays. For the MGS-1 samples, the only clay that enhanced Li sorption compared to the MGS-1 baseline (i.e., column A) was talc; the average nontronite sample also had slightly more Li sorbed, however this difference was not found to be statistically significant. a.u. = arbitrary units.

investigate the degree to which Li sorbed to different mineral matrices. The A columns were either filled with MGS-1 simulant or glass beads and the B columns contained a mixture of a clay mineral and either the glass beads or MGS-1 to simulate clay capping at the surface. Generally, we found that the glass beads was not nearly as efficient as MGS-1 simulant. Although there does appear to be a slight increase in the overall distribution of Li sorbed in column A vs B of the MGS-1 simulant (i.e., "None" in Fig. 11) this difference was not statistically significant (p = 0.24). There was some variability in the A columns containing only MGS-1 simulant amongst all the experiments, which we would expect to be minimal since they are essentially experimental replicates. Indeed, these differences were not statistically significant with the exception of nontronite (p = 0.003). Illite and nontronite in the B columns sorbed more Li than the glass beads from the corresponding A columns. However, for the MGS-1 experiments, a significant difference in Li sorption was not observed when MGS-1 in column B was partially replaced with illite (p = 0.57), nontronite (p = 0.85), an illite/smectite mixture (p = 0.85), or saponite (p = 0.72), which suggests these clays were equally efficient at sorbing Li compared to the base MGS-1 simulant. The LIBS peak area for Li decreased when kaolinite was mixed into the column with MGS-1 simulant (i.e., the peak area for column B was less than column A which only had MGS-1 simulant; Fig. 10). The decrease in the Li peak area suggests that kaolinite was *less* efficient than the MGS-1 simulant at sorbing Li (p=0.03). The only mineral found to have sorbed more Li than the MGS-1 simulant was talc (p=0.05).

With our experimental setup the A columns would undergo more exposure to the LiCl solution compared to the B columns (with the bottom of the A column being the most exposed). Accordingly, we did see an increase in the median of the normalized Li peak area in column A compared to column B of the MGS-1 control lacking clays in Fig. 11. Given these observations, a more apt comparison for determining whether clays enhance Li sorption compared to the martian regolith would be to compare the Column B sample of the MGS-1 control lacking clays with those having clays (Fig. 12). With this comparison we once again found that kaolinite was less efficient (p = 0.004) whereas talc was more efficient (p = 0.05) than the base regolith at sorbing Li, respectively. However, unlike our previous observations, we also found that the enhanced Li sorption brought by illite was statistically significant (p = 0.03). Accordingly, the experiment with the illite/smectite mixture also increased the median Li sorbed and this difference was close to being considered significant (p = 0.08).

3.1.4. Deducing the mechanism for Li sorption

To deduce the mechanism by which Li was being added to the system

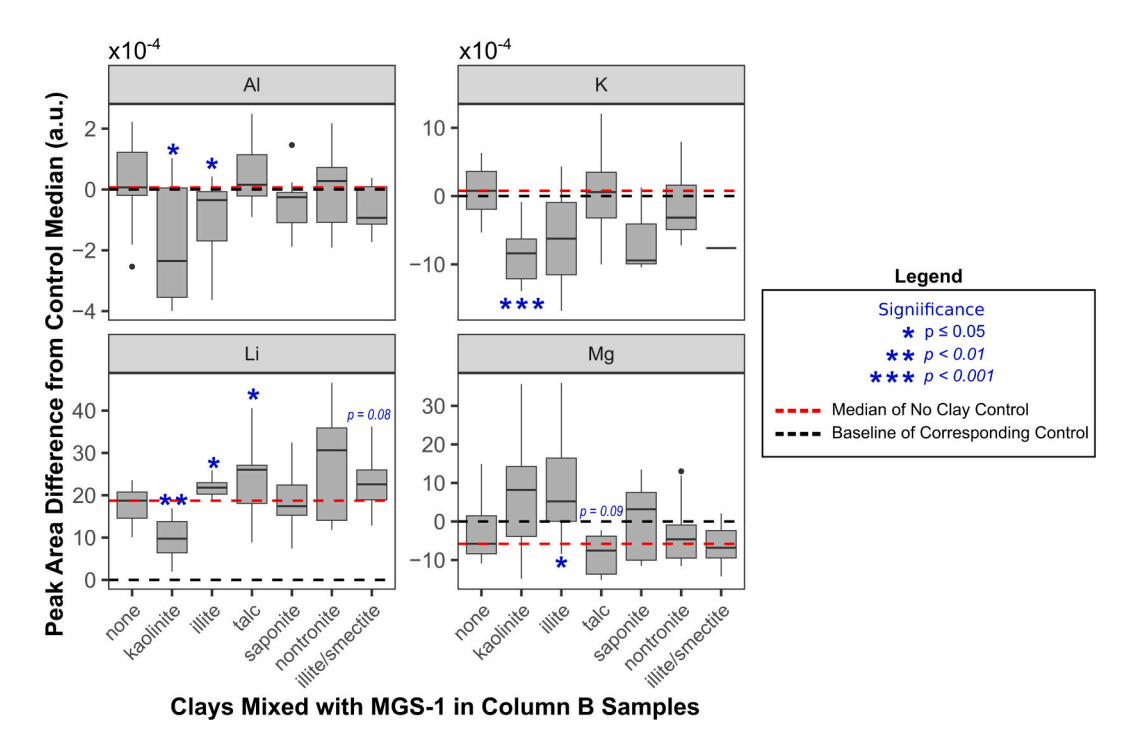


Fig. 12. Elemental analysis of experiments exposed to LiCl. Plotted is the difference in Al, K, Li, and Mg peak areas observed by LiBS between mineral matrices (i.e. column B) exposed to a flowing solution of 100 mM Li and the corresponding control that was exposed to pure water (i.e. column B of the same experimental set up in Fig. 10). The red dashed line represents the median value of the sample lacking clays (i.e. "none" on the plot) and is drawn to facilitate comparisons of adding different clays to column B. The black dashed line represents the baseline from the corresponding control (i.e. no change after exposure to LiCl). Elemental abundance impacted by Li sorption by the clays must be different than both the control lacking clays (red dashed line) and the corresponding clay experiment not exposed to LiCl (black dashed line). Statistical significance in the difference between adding clay vs no clay is denoted with a blue asterisk. a.u. = arbitrary units. (For interpretation of the references to colour in this figure legend, the reader is referred to the web version of this article.)

Table 2
Elemental Chemistry of Clays and Experimental Samples. Shown is the elemental composition (oxide wt%) expected for each Column B experiments containing a 50/50 mixture of MGS-1 and a clay. Note, unlike Table 1 the values are not normalized to 100 %. For the elemental composition of each source clay see Table S1; abundances were reported by the source vendor. All clays have values reported except talc and saponite which were not measured by the vendor and were synthesized for this work, respectively. Thus, for this experiment we report estimated values of talc based on its chemical formula; for saponite we provide a qualitative description of whether we expect the elemental signal to be high (hi) or low (lo/low) in the LIBS spectra based on the general chemical formula. The values for the elements are colored relative to each

Mineral	Chemical Formula	Al ₂ O ₃	Na ₂ O	CaO	MgO	K ₂ O	FeOT	SiO ₂
MGS-1	Mineral mixture	14.7	1.8	8.9	15.5	0.6	11.7	44.7
Kaolinite	Al ₂ Si ₂ O ₅ (OH) ₄	27.2	0.9	4.4	7.8	0.3	5.9	44.5
Illite	(K,H ₃ O)•(Al, Mg, Fe) ₂ •(Si Al) ₄ •O ₁₀ •[(OH) ₂ , (H ₂ O)]	19.5	0.9	4.7	9.0	4.2	9.4	47.0
Talc	Mg ₃ Si ₄ O ₁₀ (OH) ₂	~7.4	~0.9	~4.4	~23.7	~0.3	~5.8	~54.1
Saponite	Ca _{0.25} (Mg,Fe) ₃ ((Si,Al) ₄ O ₁₀)(OH) ₂ ·n(H ₂ O)	Hi-Lo	Low	Low	Hi-Lo	Low	Hi-Lo	Hi-Lo
Nontronite	(CaO _{0.5} ,Na) _{0.3} Fe ³⁺ ₂ (Si,Al) ₄ O ₁₀ (OH) ₂ ·nH ₂ O)	9.1	0.9	5.8	7.9	0.3	22.7	50.9
Illite/Smectite	Mineral mixture	20.2	1.0	4.8	9.0	3.0	6.3	48.2

column (green = highest values, yellow = lowest values, white = no data).

(i.e., via replacement of alternative cations or precipitation on the surface as the solution dried) we investigated the changes in the elemental composition of each glass and MGS-1 experiment exposed to LiCl solution. Given that glass was not an efficient sorbent for Li (Fig. 11), any changes in the elemental chemistry after adding clays and exposing to LiCl could be attributed to Li sorption by the clays of interest. Fig. S5 shows the elemental chemistry of the glass experiments when exposed to water or LiCl (column B – top only). We observed that Li sorption by illite and nontronite correlated with a statistically significant increase in Al and Mg (for both clays re. Al: p < 0.001 and re. Mg: p < 0.005 compared to their corresponding water exposed control). For the glass beads control Li sorption correlated with a decrease in both Al (p = 0.15) and Mg (p = 0.01), though only the Mg change was considered

statistically significant. Moreover, Li sorption correlated with a drop in K levels for all three samples, with no K being detected in the illite sample; K levels for nontronite lowered to the levels of the glass beads control (i. e. there was no statistical difference between the values: p=0.4). Notably, glass beads with illite had the highest levels of K (p<0.001 compared to nontronite and the glass control), followed by nontronite (p<0.001 compared to the glass control) and both were more enriched in K than the glass beads control (Fig. S3), thus the non detection of K in the illite sample is significant. Further evidence supporting the relationship between these elements and Li sorption stems from the fact that the changes in Al, Mg, and K were proportional to the amount by which Li was sorbed by illite, nontronite, and the glass beads control (Fig. 11). Indeed, illite (having sorbed the most Li) also had the most significant

increase in Al and Mg and most signficiant decrease in K. All together, these observations suggest that Li is replacing Al and Mg in the glass beads whereas for the clays Li is replacing K. The liberated Al and Mg from the glass beads could then explain the increase in Al and Mg within the upper clay containing columns: cations (including K) within the clays could be undergoing cation exchange with the Al and Mg stemming from the bottom column. To test this hypothesis, we investigated changes in the elemental composition between columns A (bottom, glass beads only) and B (glass beads with clay) for the LiCl solution (Fig. S6). Consistent with our hypothesis we confirmed that Al and Mg were indeed less prevalent in the bottom columns (A) for the experimental set up containing illite (p < 0.001) and nontronite (p = 0.002); the difference in Al between the A and B columns for the glass beads control was not statistically signficant as expected given that there are no clays in the B column to faciliate the resorption of the liberated Al from the A column (p = 0.84). In contrast, K levels were higher within the bottom (A) columns compared to the depleted top columns (B) for each experiment (Fig. S6).

We then explored what the elemental changes in the MGS-1 experiemnts could tell us about Li sorption, espcially given that more clays were studied with this set up. As shown in Fig. 12 the Li content for all the samples increased compared to the water controls. If the increase in Li was solely due to the precipitation of LiCl as the solution dried, we would expect the signal for all the elements to decrease proportionally. However, this was not the case. For the MGS-1 control lacking clay, we observed a slight decrease in Mg when the MGS-1 control was exposed to LiCl compared to pure water (p = 0.08). This suggests that part of the mechanism for Li sorption for MGS-1 is via replacement of Mg ions. Accordingly, the Mg signal was found to be significantly less in the bottom column (A) compared to the top column (B) of the experimental set containing illite. For talc, we also observed a decrease in the Mg signal compared to the corresponding water control (p = 0.05); accordingly, the decrease in Mg within the talc sample compared to the MGS-1 control exposed to LiCl is near statistical significance (p = 0.09). In contrast, the Mg signal increased (in agreement with the glass experiments) for the illite sample compared to the MGS-1 control exposed to LiCl (p = 0.02); the Mg signal within illite exposed to LiCl was also higher than the Mg signal in an illite sample exposed to water (though this was not found to be statistically significant; Fig. S7). Rather than Mg, the Al and K signals decreased for illite compared to the MGS-1 control (p = 0.03 for Al); this was also in agreement with the glass experiments. Finally, experiments with kaolinite that were exposed to LiCl had (compared to the MGS-1 control) less Al (p = 0.01) and K (p < 0.01) 0.001), but an increase in Mg (p = 0.14); these trends were also observed when comparing kaolinite samples exposed to LiCl to the corresponding kaolinite sample exposed to water (Al: p = 0.07; K: p = 0.014; Mg: p =

Overall, our interpretations of Li sorption deduced from the glass experiments are consistent with observations from the MGS-1 experiments, bolstering our confidence in the observed trends and proposed mechanism. Our evidence suggests that Li replaces Al and Mg in the glass beads and Mg in MGS-1, both of which result in an increase in these elements in the top column where they can then undergo cation substitution within the clays present (vs leaving the system). Accordingly, Al was more prominent for illite after exposure to LiCl only in the glass bead experiments, whereas the Mg signal was more prominent in the illite samples for both the glass and MGS-1 experiments. For the illite and kaolinite samples it appears that exposing the mineral mixtures to LiCl increased the amount of Mg in the B (top) columns containing the clay. This suggests that Li is not replacing Mg within either of these clays; in fact, Mg released from the bottom column containing MGS-1 may be substituting other ions in each clay (increasing the amount of Mg in the sample); indeed, Mg substitution for Al is a known phenomenon for kaolinite. Rather, Li may be replacing sorbed K within illite and kaolinite samples; Li may also be substituting for Al, however the decrease in Al may also be due to Mg substitution. These results are not surprising given that illite and kaolinite have relatively little Mg and are the most enriched in Al and K whereas MGS-1 and talc have the highest Mg levels (Table 2; Fig. S3). Notably, cation substitution is relatively limited for kaolinite compared to the other clays used in this study because it has a 1:1 structure that does not lend itself to the formation of frayed edge sites that can promote cation sorption and exchange. Moreover, the kaolinite used in our work was already relatively enriched in Li which may have limited the degree to which additional Li could be substituted into the clay. Like kaolinite, illite and talc are both nonswelling clays; however, unlike kaolinite these are 2:1 clays whose outer layers can form frayed edge sites (via substitution of K with larger cations such as hydrated Ca). These frayed sites can promote the sorption of other cations including Li; cation exchange can also occur within the interlayers. The 2:1 swelling clays (saponite, nontronite, smectite) are likely not as efficient at sorbing Li because of their ability to significantly expand upon hydration – thus Li may have to compete with additional cations dissolved in the water including hydronium ions and water molecules.

3.2. Reflectance spectra

Reflectance spectra of the experiments with MGS-1 showed no major changes in clay mineralogy induced by the experiment (Fig. S1). Reflectance spectra of the experiments with glass beads as the simulant showed no major changes in clay mineralogy induced by the experiment except for in the saponite experiment the metal-OH absorption appears to shift to slightly shorter wavelengths in the post-experiment column B sample (Fig. S2).

4. Discussion

4.1. Observations in laboratory experiments

We observed that the metal-OH absorption in VNIR reflectance spectra shifted to slightly shorter wavelengths in the post-experiment packed bed B sample of the saponite glass bead experiment exposed to Li, which could suggest oxidation of the Fe²⁺ in the saponite (Fig. S2).

Our experiments with the glass beads show that nontronite and illite both enhanced Li sorption. We found that talc was capable of pulling Li from groundwater simulant into the solid sample (Figs. 11, 12) and that this enhanced sorption could be detectable by LIBS when comparing deeper sediments (that may be more exposed to LiCl solutions i.e. column A) with upper sediments capped by talc (i.e. column B, Fig. 11). Furthermore, our work suggests that in addition to talc, illite is also more efficient than the base MGS-1 simulant at sorbing Li (Fig. 12). In other words, Li can be a tracer for sediments relatively enriched in talc or illite. Whether this was via incorporation into the mineral structure or surface adsorption, this finding supports the observation that Li moves with some clay minerals (here talc) in Gale crater and may be a suitable proxy for specific types of clay minerals in rocks affected by aqueous diagenetic processes. Both clays tested (illite and nontronite) exhibited higher lithium (Li) sorption capacity compared to the glass beads, however, their Li adsorption showed no statistically significant difference from the MGS-1-only column (A). This observation does not preclude the possibility that Li could be indicative of an enrichment of nontronite. Indeed, via LIBS we observed that the median Li peak area increased after mixing nontronite to the MGS-1 column. The high variability in LIBS observations prevents us from confidently concluding that this difference is statistically significant. Notably, ChemCam typically acquires 30 laser shots per point, each which generates its own individual spectrum. In contrast, the JPL LIBS continuously collects light while the 250 shots are acquired. Consequently, the resulting LIBS spectrum from the JPL LIBS may be more susceptible to noise and fluctuations in the laser. Given this, subtle changes in Li may be easier to detect with ChemCam compared to our LIBS instrument. Given this, we would recommend that future work prioritize testing whether Li could

be a tracer of both talc and nontronite. We also recommend the development of a calibration curve for measuring Li in martian samples via ChemCam, such a calibration could further improve the team's ability to discern the significance in changes of Li observed by LIBS.

4.2. Implications for Gale crater

The types of clay minerals identified in Gale crater via CheMin include smectite, illite, and kaolinite (Bristow et al., 2015, 2018a, b; Rampe et al., 2020a, 2020b; Tu et al., 2021). Smectites generally indicate the presence of neutral to alkaline conditions and suggest that water was available for prolonged periods; however, recent studies, such as Peretyazhko et al. (2018), demonstrate that smectites can also form under acidic conditions on Mars, particularly in environments influenced by volcanic activity and sulfuric acid, thus broadening the possible environmental contexts in which these minerals can form. The presence of smectites also suggests that water was available for prolonged periods, allowing for extensive chemical weathering. Illites, on the other hand, are non-expandable clays that typically form under slightly acidic to neutral conditions and can indicate more moderate weathering processes or diagenetic processes (i.e., illitization). Kaolinites are indicative of acidic conditions and intense weathering, usually in a relatively warm and wet environment (Allen and Scheid, 1946; Sherman, 1952; Barshad, 1966; Baker and Strawn, 2014).

In the VRR region (Fig. 2), where the Li-clay mineral content relationship was proposed, CheMin observed peaks consistent with dioctahedral collapsed smectites (Table 3). A ~ 9.6 Å peak in High Field and Rock Hall has been attributed to ferripyrophyllite (Tu et al., 2021). In addition, a 9.2 Å peak observed in the Aberlady and Kilmarie samples was modeled as mixed-layer talc-serpentine when viewed in conjunction with elemental abundance data from the alpha-particle X-ray spectrometer (APXS) instrument (Bristow et al., 2021; Tu et al., 2021; Thorpe et al., 2022).

Furthermore, the trend has been noted that, around Vera Rubin ridge, low-Li ChemCam targets are low in clay mineral content in XRD

Table 3 CheMin results from the drill holes shown in Fig. 2.

Drill site	001 d- spacing	021 d- spacing	Interpretation	Reference
Duluth	~10 Å	4.5 Å	First fully dioctahedral smectite detected	Rampe et al. (2020a, 2020b); Thorpe et al. (2022)
Stoer	~10 Å	4.5 Å	Fe ³⁺ -rich dioctahedral. Collapsed smectite or ferripyrophyllite	Rampe et al. (2020a, 2020b); McAdam et al. (2020)
High Field	~9.6 Å	4.5 Å	Fe ³⁺ -rich dioctahedral. Collapsed smectite or ferripyrophyllite	Rampe et al. (2020a, 2020b); McAdam et al. (2020)
Rock Hall	~9.6 Å	4.5 Å	Fe ³⁺ -rich dioctahedral. Collapsed smectite or ferripyrophyllite	Rampe et al. (2020a, 2020b); McAdam et al. (2020)
Aberlady	~9.22, 10 Å	4.5 Å	10 Å due to collapsed smectite, 9.22 due to mixed-layer talc- serpentine	Bristow et al. (2021); Tu et al. (2021); Thorpe et al. (2022)
Kilmarie	~9.22, 10 Å	4.5 Å	10 Å due to collapsed smectite, 9.22 due to mixed-layer talc- serpentine	Bristow et al. (2021); Thorpe et al. (2022)
Glen Etive	~10 Å	4.5 Å	Collapsed smectite	Bristow et al. (2021); Thorpe et al. (2022)
Glen Etive 2	~10 Å	4.5 Å	Collapsed smectite	Bristow et al. (2021); Thorpe et al. (2022)

and that high-Li ChemCam targets are high in clay mineral content (Frydenvang et al., 2020; Bristow et al., 2021; Dehouck et al., 2022). We extend this to say specifically that the Aberlady and Kilmarie samples have noted talc content (Bristow et al., 2021; Tu et al., 2021) and the highest Li content in this area (Fig. 2). Therefore, it is possible that talc in particular is the clay mineral driving the Li-clay mineral trend in the VRR region of Gale crater. Future CheMin investigations that identify a 9.2 Å peak should examine the Li content of the bedrock using ChemCam LIBS to test whether this relationship holds in different environments.

We envision two possible pathways of formation of Li-enriched talc in Glen Torridon, especially at Aberlady and Kilmarie. In the first, alkaline Li-bearing hydrothermal (50-200 °C) groundwater flows through GT precipitating Li-bearing talc from Mg-rich precursors. This may represent a modified version of the hydrothermal alteration precipitating talc proposed in Brown et al. (2010) and Viviano et al. (2013) where alteration of serpentine forms talc and carbonate. This may be consistent with CheMin's observations of mixed-layer talc-serpentine in both samples, as well as the carbonate siderite in Kilmarie (Morrison et al., 2024).

In the second, pre-existing talc or illite is exposed to Li-bearing diagenetic groundwater and incorporates it. This is perhaps consistent with the impermeable nature of Glen Torridon. Late-stage diagenetic fluids are known to have moved through VRR, coarsening the hematite grains found there (Fraeman et al., 2020). Adjacent to VRR, Glen Torridon is notably lacking in diagenetic nodules compared to the rest of Mt. Sharp. Glen Torridon's high clay mineral content may have formed an aquitard limiting the access of the area to diagenetic fluids directed there by the coarse-grained Greenheugh Pediment, perhaps increasing alteration of nearby areas including VRR (Rudolph et al., 2022; Ando et al., 2025).

Possible complicating factors to the link we propose here between elevated Li and talc or illite content include (i) imperfect or incomplete identification on Mars, (ii) inter-clay transformation, (iii) other clay minerals could absorb Li under untested conditions, and (iv) primary incorporation of Li during clay formation. (i) It is possible that talc or illite is more widespread within Gale crater and has not been confidently identified using CheMin due to low abundance or limitations in the XRD signal. In this scenario, the correlation between Li and talc would be either accidental or caused by a separate process that increased talc abundance or XRD pattern clarity as well as Li content. (ii) It is possible that some clay minerals identified by the rover may have originally had another mineral form and have since transformed into talc or illite by another process. Inter-clay transformations are common in sedimentary and hydrothermal environments, particularly where fluid composition, temperature, or water:rock ratios change over time (). In this case, the current mineralogy detected by CheMin would reflect a diagenetically overprinted signature, potentially obscuring the original Li-hosting phase. Li may have been structurally incorporated into talc during early diagenesis and retained through subsequent mineral transformations. Thus, the present-day clay assemblage may not directly reflect the original mineral host responsible for Li sorption. (iii) It is also possible that conditions other than those tested by our experiments could lead to other clays absorbing Li on Mars, but only talc responds to the conditions we tested. If the fluids on Mars had a different pH or temperature than we test in the laboratory, it is possible other clays would have incorporated Li and talc not so. Therefore, the lack of significant Li sorption in some clays (compared to MGS-1) under our experimental conditions does not eliminate their potential to host Li in natural martian settings. (iv) Finally, elevated Li in talc in Gale crater could be due to primary formation conditions leading to elevated Li rather than groundwater exposure. In this scenario, the Li-clay correlation in Gale crater would reflect a primary igneous or hydrothermal signature rather than diagenetic or weathering processes.

Ultimately, while our results suggest that talc and illite are efficient at Li sorption under Mars-relevant conditions, it is possibly one of multiple contributors to the elevated Li observed across VRR. A

combination of processes may have led to the coexisting elevated talc and Li abundances in Aberlady and Kilmarie, in particular.

Areas for future work include collection of XRD patterns for more direct comparison with CheMin data, as well as efforts to confirm which type of sorption are responsible for this change (e.g., Fig. 1).

Clay minerals are a main focus of the Mars Science Laboratory mission as they are one of the most common secondary minerals on Mars, their formation requires water, their structure can trap and bind organics, and they dominate the most ancient martian terrains that formed while Earth was first evolving life. Identifying elements that can act as proxies for clay mineral content is very valuable to the search for habitable environments and those that encourage preservation of any past biomarkers. Our findings support the interpretation of Li as a talc proxy in Gale crater and put forth that talc in martian rocks may be effective at removing Li from martian groundwater.

Of the clays used in this study, talc was the only one found to have a statistically significant boost in Li sorption as detectable by LIBS when directly comparing to MGS-1 simulant and bottom sediments that are likely to have undergone additional exposure to Li from groundwaters. Notably, of the clays used in this study talc is the most relevant for astrobiology given that it is often associated with serpentine and, accordingly, is formed via hydrothermal serpentinization reactions involving olivine (Bristow et al., 2021; Tu et al., 2021); illite and illitesmectite mixtures can also be byproducts of secondary alteration of serpentinites. Serpentinization, which also generates H2 and pH gradients that could be harnessed to drive chemical reactions, is especially interesting in the context of abiotic organic synthesis and habitability (Russell et al., 2010; Holm et al., 2015). The resulting H₂ could act as a reductant for abiotic organic synthesis, including CO and CO2 reduction to methane and other organic compounds via Fischer Tropsch Type (FTT) synthesis reactions (Rodriguez et al., 2024). Thus, Li, being a potential proxy for talc and thus serpentinization could prove to be an exciting tracer for identifying astrobiologically interesting targets for subsequent analysis by Curiosity and for caching for future sample return by the Perseverance rover.

5. Conclusions

Li has been proposed as a clay mineral proxy in Gale crater based on observations of elevated Li and clay mineral content in Vera Rubin ridge (Frydenvang et al., 2020; Bristow et al., 2021; Dehouck et al., 2022). We conducted continuous flow reactor experiments to examine how Li content of Mars-relevant clay minerals and MGS-1 Mars simulant would change when exposed to fluids with elevated Li content. We observed that column packed beds that contained talc showed statistically significant elevated Li content after exposed to Li-bearing fluid, compared to when exposed to pure water. The drilled samples in Gale crater at Aberladie and Kilmarie have the highest Li content and XRD peaks at 9.2 Å that have been attributed to talc (Bristow et al., 2021; Tu et al., 2021). Given these results, this proposed trend of Li as a clay mineral proxy may be specific to talc. This is an important distinction as XRD observations on Mars are time-intensive to acquire, while VNIR reflectance spectroscopy and elemental abundance data (e.g. LIBS) are relatively faster and therefore more frequently collected. Our experimental results imply that we can get a more complete perspective of the clay mineralogy of an area on Mars from VNIR or LIBS analysis, particularly if it may contain talc or illite. This is important as talc not only requires water to form but may be related to hydrothermal or serpentinization processes which are astrobiologically important.

CRediT authorship contribution statement

Rachel Y. Sheppard: Writing – review & editing, Writing – original draft, Project administration, Methodology, Investigation, Conceptualization. Jessica M. Weber: Writing – review & editing, Supervision, Project administration, Methodology, Funding acquisition. Laura E.

Rodriguez: Data curation, Writing – review & editing, Writing – original draft, Methodology, Investigation. Cathy Trejo: Writing – review & editing, Investigation, Data curation. Elisabeth M. Hausrath: Writing – review & editing, Investigation, Data curation. Laura M. Barge: Writing – review & editing, Supervision, Funding acquisition.

Declaration of competing interest

The authors declare that they have no known competing financial interests or personal relationships that could have appeared to influence the work reported in this paper.

Acknowledgments

We would like to thank Bethany Ehlmann for the IMt-2 illite sample provided by her laboratory. We would like to thank the HiRISE team and the CheMin, and ChemCam teams from the Mars Science Laboratory mission for collecting and processing the data used here. We would like to thank Bonnie Teece for student advising, and assistance with experiments and data interpretation. We would like to acknowledge funding from the Mars Science Laboratory Participating Scientist Program. RYS was funded as a MSL Participating Scientist (grant # 80NSSC23K0189). LMB was funded as a MSL Participating Scientist; the research was carried out at the Jet Propulsion Laboratory, California Institute of Technology, under a contract with the National Aeronautics and Space Administration (80NM0018D0004). EMH was funded as a MSL Participating Scientist (grant # 80NSSC22K0656). LER was funded as a MSL Participating Scientist (grant #80NSSC23K0190) and by LPI which is operated by USRA under a cooperative agreement with the Science Mission Directorate of the National Aeronautics and Space Administration. JMW was funded by a JPL Spontaneous Research and Development Award. The research was carried out at the Jet Propulsion Laboratory, California Institute of Technology, under a contract with the National Aeronautics and Space Administration (80NM0018D0004).

Appendix A. Supplementary data

Supplementary data to this article can be found online at https://doi.org/10.1016/j.icarus.2025.116769.

Data availability statement

Filename: LIBS_prepocessed.CSV

Pre-processed LIBS data corresponding to each measurement made for each sample are provided as a single CSV with each row corresponding to a single measurement from a particular experiment. The columns provide details about the sample: the experiment, column (dry standard, A, or B), with what the column was packed (glass beads, MGS-1, clay and glass beads, or clay and MGS-1), the specific clay within the packed bed, clay structure, clay type, the composition of the fluid (i.e. "water"), the LIBS parameters (SR, SI, number of shots), the point analyzed per sample, and finally the rest of the columns correspond to intensity measured at each LIBS wavelength (nm).

Filename: Deconvolved_peak_areas.CSV

This file contains all of the peak areas deconvolved using the script described in the manuscript. Each row corresponds to a particular measurement for a single sample. The columns correspond peak area corresponding to each element (Li, Fe, Mg, Si, Al, Ca, Na, K) and the error affiliated with the corresponding fit followed by the experimental parameters (see description for the LIBS file for details).

Supplementary_Data.doc

This document includes text describing the elemental distributions observed in the glass bead experiments exposed to water. Also included is Table S1 which summarizes the elemental chemistry of the source clays and box plots showing LIBS results in Figs. S1-S6.

References

- Ajouyed, O., Hurel, C., Ammari, M., Marmier, N., 2011. Sorption of lithium on smectite and kaolinite. J. Hazard. Mater. 194, 62–68. https://doi.org/10.1016/j. jhazmat.2011.07.080.
- Allen, V.T., Scheid, V.E., 1946. Nontronite in the Columbia River region. Am. Mineral. 31, 294–312.
- Ando, J., Sheppard, R.Y., Bryk, A.B., Sun, V., Seeger, C.H., Fraeman, A.A., Eng, A.M., Kah, L., Rudolph, A.N., 2025. Diagenetic features reveal the influence of the Greenheugh Pediment on the alteration history of Gale crater, Mars. J. Geophys. Res. Planets 130, e2024JE008891. https://doi.org/10.1029/2024JE008891.
- Ashry, M.M., 1973. Geochemical behavior of lithium in clay minerals. Geochim. Cosmochim. Acta 37 (10), 2449–2458. https://doi.org/10.1016/0016-7037(73) 90120-1.
- Baker, L.L., Strawn, D.G., 2014. Temperature Effects on the Crystallinity of Synthetic Nontronite and Implications for Nontronite.
- Baldermann, A., Dohrmann, R., Kaufhold, S., Nickel, C., Mavromatis, V., 2018. The Fe-Mg-saponite solid solution series—a hydrothermal synthesis study. Am. Mineral. 103 (7), 1096–1107. https://doi.org/10.2138/am-2018-6354.
- Barshad, I., 1966. The effect of a variation in precipitation on the nature of clay mineral formation in soils from acid and basic igneous rocks. Proc. Int. Clay Conf. 167–173.
- Benson, T.R., Coble, M.A., Rytuba, J.J., Mahood, G.A., 2017. Lithium enrichment in rhyolite magmas of intracontinental calderas. Nat. Commun. 8, 270. https://doi.org/ 10.1038/s41467-017-00234-y.
- Bristow, T.F., Bish, D.L., Vaniman, D.T., Morris, R.V., Blake, D.F., Grotzinger, J.P., Farmer, J.D., 2015. The origin and implications of clay minerals from Yellowknife Bay, Gale crater, Mars. Am. Mineral. 100 (4), 824–836. https://doi.org/10.2138/am-2015-5077CCBYNCND.
- Bristow, T.F., Haberle, R.M., Blake, D.F., Rampe, E.B., Achilles, C.N., Siebach, K.L., 2018a. Clay mineralogy and the influence of organic carbon preservation in Gale Crater sediments, Mars. J. Geophys. Res. 123 (7), 1825–1850. https://doi.org/ 10.1029/2018JE005602.
- Bristow, T.F., Rampe, E.B., Achilles, C.N., Blake, D.F., Chipera, S.J., Craig, P., Crisp, J.A., Des Marais, D.J., Downs, R.T., Gellert, R., Grotzinger, J.P., Gupta, S., Hazen, R.M., Horgan, B., Hogancamp, J.V., Mangold, N., Mahaffy, P.R., McAdam, A.C., Ming, D. W., Morookian, J.M., Morris, R.V., Morrison, S.M., Treiman, A.H., Vaniman, D.T., Vasavada, A.R., Yen, A.S., 2018b. Clay mineral diversity and abundance in sedimentary rocks of Gale crater, Mars. Sci. Adv. 4, eaar3330.
- Bristow, T.F., Grotzinger, J.P., Rampe, E.B., Cuadros, J., Chipera, S.J., Downs, G.W., Fedo, C.M., Frydenvang, J., McAdam, A.C., Morris, R.V., Achilles, C.N., Blake, D.F., 2021. Brine-driven destruction of clay minerals in Gale crater, Mars. Science 372 (6546), 956–961. https://doi.org/10.1126/science.abg5449.
- Brown, A.J., Hook, S.J., Baldridge, A.M., Crowley, J.K., Bridges, N.T., Thomson, B.J., Marion, G.M., de Souza Filho, C.R., Bishop, J.L., 2010. Hydrothermal formation of clay-carbonate alteration assemblages in the Nili Fossae region of Mars. Earth Planet. Sci. Lett. 297. 174–182.
- Cannon, K.M., Britt, D.T., Smith, T.M., Fritsche, R.F., Batcheldor, D., 2019. Mars global simulant MGS-1: a Rocknest-based open standard for basaltic Martian regolith simulants. Icarus 317, 470–478.
- Chemtob, S.M., Nickerson, R.D., Morris, R.V., Agresti, D.G., Catalano, J.G., 2015. Synthesis and structural characterization of ferrous trioctahedral smectites: implications for clay mineral genesis and detectability on Mars. J. Geophys. Res. Planets 120, 1119–1140. https://doi.org/10.1002/2014JE004763.
- Constantine, W., Percival, D., 2017. Wavelet Methods for Time Series Analysis. https://gi thub.com/cran/wmtsa.
- Decarreau, A., et al., 2008. Hydrothermal synthesis, between 75 and 150 C, of highcharge, ferric nontronites. Clay Clay Miner. 56, 322–337.
- Dehouck, E., Rapin, W., McAdam, A.C., Bish, D.L., Thorpe, M.T., Achilles, C.N., Bristow, T.F., Rampe, E.B., MSL Science Team, 2022. Clay mineral diversity and abundance in sedimentary rocks of Gale Crater, Mars. J. Geophys. Res.: Planets 127 (6), e2021JE007098. https://doi.org/10.1029/2021JE007098.
- Dugamin, E.J.M., Richard, A., Cathelineau, M., et al., 2021. Groundwater in sedimentary basins as potential lithium resource: a global prospective study. Sci. Rep. 11, 21091. https://doi.org/10.1038/s41598-021-99912-7.
- Edgar, L.A., Gupta, S., Rubin, D.M., Lewis, K.W., et al., 2017. Shaler: in situ analysis of a fluvial sedimentary deposit on Mars. Sedimentology 65, 96–122.
- Elzhov T.V., Mullen K.M., Spiess A., Bolker B. (2023). _minpack.lm: R Interface to the Levenberg-Marquardt Nonlinear Least-Squares Algorithm Found in MINPACK, Plus Support for Bounds. R package version 1.2-4, https://CRAN.R-project.org/package=minpack.lm.
- Fairén, A.G., Davila, A.F., Gago-Duport, L., Amils, R., McKay, C.P., 2015. Stability against freezing of aqueous solutions on early Mars. Nat. Geosci. 8, 688–691. https://doi. org/10.1038/ngeo2543.
- Fedo, C.M., Bryk, A.B., Edgar, L.A., Bennett, K.A., Fox, V.K., Dietrich, W.E., et al., 2022. Geology and stratigraphic correlation of the Murray and Carolyn shoemaker formations across the Glen Torridon region, Gale crater, Mars. J. Geophys. Res. 127, e2022JE007408. https://doi.org/10.1029/2022JE007408.
- Fraeman, A.A., Edgar, L.A., Rampe, E.B., Thompson, L.M., Frydenvang, J., Fedo, C.M., et al., 2020. Evidence for a diagenetic origin of Vera Rubin ridge, Gale crater, Mars: summary and synthesis of curiosity's exploration campaign. J. Geophys. Res. 125, e2020JE006527. https://doi.org/10.1029/2020JE006527.
- Frydenvang, J., Mangold, N., Wiens, R.C., Fraeman, A.A., Edgar, L.A., Fedo, C.M., et al., 2020. The Chemostratigraphy of the Murray formation and role of diagenesis at Vera Rubin ridge in Gale Crater, Mars, as observed by the ChemCam instrument. J. Geophys. Res. 125 (9), e2019JE006320. https://doi.org/10.1029/2019JE006320.

- Grotzinger, J.P., Sumner, D.Y., Kah, L.C., Stack, K., Gupta, S., Edgar, L., Rubin, D., Lewis, K., Schieber, J., Mangold, N., Milliken, R., Conrad, P.G., DesMarais, D., Farmer, J., Siebach, K., Calef, F., Hurowitz, J., McLennan, S.M., Ming, D., Vaniman, D., Crisp, J., Vasavada, A., Edgett, K.S., Malin, M., Blake, D., Gellert, R., Mahaffy, P., Wiens, R.C., Maurice, S., Grant, J.A., Wilson, S., Anderson, R.C., Beegle, L., Arvidson, R., Hallet, B., Sletten, R.S., Rice, M., Bell, J., Griffes, J., Ehlmann, B., Anderson, R.B., Bristow, T.F., Dietrich, W.E., Dromart, G., Eigenbrode, J., Fraeman, A., Hardgrove, C., Herkenhoff, K., Jandura, L., Kocurek, G., Lee, S., Leshin, L.A., Leveille, R., Limonadi, D., Maki, J., McCloskey, S., Meyer, M., Minitti, M., Newsom, H., Oehler, D., Okon, A., Palucis, M., Parker, T., Rowland, S., Schmidt, M., Squyres, S., Steele, A., Stolper, E., Summons, R., Treiman, A., Williams, R., Yingst, A., the MSL Science Team, 2014. A habitable fluvio-lacustrine environment at Yellowknife bay, Gale Crater, Mars. Science 343, 1242777.
- Gainey, S.R., Hausrath, E.M., Adcock, C.T., Tschauner, O., Hurowitz, J.A., Ehlmann, B.L., Xiao, Y., Bartlett, C.L., 2017. Clay mineral formation under oxidized conditions and implications for paleoenvironments and organic preservation on Mars. Nat. Commun. 8, 1230.
- Grotzinger, J.P., Gupta, S., Malin, M.C., Rubin, D.M., Schieber, J., Siebach, K., Sumner, D.Y., Stack, K.M., Vasavada, A.R., Arvidson, R.E., Calef, F., Edgar, L., Fischer, W.F., Grant, J.A., Griffes, J., Kah, L.C., Lamb, M.P., Lewis, K.W., Mangold, N., Minitti, M.E., Palucis, M., Rice, M., Williams, R.M.E., Yingst, R.A., Blake, D., Blaney, D., Conrad, P., Crisp, J., Dietrich, W.E., Dromart, G., Edgett, K.S., Ewing, R.C., Gellert, R., Hurowitz, J.A., Kocurek, G., Mahaffy, P., McBride, M.J., McLennan, S.M., Mischna, M., Ming, D., Milliken, R., Newsom, H., Oehler, D., Parker, T.J., Vaniman, D., Wiens, R.C., Wilson, S.A., 2015. Deposition, exhumation, and paleoclimate of an ancient lake deposit, Gale crater, Mars. Science 350, aac7575.
- Holm, N.G., Oze, C., Mousis, O., Waite, J.H., Guilbert-Lepoutre, A., 2015.
 Serpentinization and the formation of H2 and CH4 on celestial bodies (planets, moons, comets). Astrobiology 15, 7. https://doi.org/10.1089/ast.2014.1188587
- Horstmann, U.E., 1957. Lithium in clay minerals. Geochim. Cosmochim. Acta 11 (4), 215–219. https://doi.org/10.1016/0016-7037(57)90025-8.
- Hurowitz, J.A., Grotzinger, J.P., Fischer, W.W., McLennan, S.M., Milliken, R.E., Stein, N., Vasavada, A.R., Blake, D.F., Dehouck, E., Eigenbrode, J.L., Fairén, A.G., Frydenvang, J., Gellert, R., Grant, J.A., Gupta, S., Herkenhoff, K.E., Ming, D.W., Rampe, E.B., Schmidt, M.E., Siebach, K.L., Stack-Morgan, K., Sumner, D.Y., Wiens, R. C., 2017. Redox stratification of an ancient lake in Gale crater, Mars. Science 356 (eaah6849).
- Liland, K.H., Almøy, T., Mevik, B.-H., 2010. Rolling-ball method for estimating the boundary of the support of a point-process intensity. J. Chemomet. 24 (7–8), 441–447.
- McAdam, A.C., Sutter, B., Archer, P.D., Franz, H.B., Wong, G.M., Lewis, J.M., Eigenbrode, J.L., Stern, J.C., Knudson, C.A., Clark, J.V. Constraints, on the Mineralogy and Geochemistry of Vera Rubin Ridge, Gale Crater, Mars, 2020. From Mars science laboratory sample analysis at Mars evolved gas analyses. J. Geophys. Res. Planets 125, e2019JE006309.
- Mizutani, T., Fukushima, Y., Okada, A., Kamigaito, O., Kobayashi, T., 1991. Synthesis of 1:1 and 2:1 iron phyllosilicates and characterization of their iron state by Mössbauer spectroscopy. Clays Clay Miner. 39, 381–386.
- Morrison, S.M., Blake, D.F., Bristow, T.F., Castle, N., Chipera, S.J., Craig, P.I., Downs, R. T., Eleish, A., Hazen, R.M., Meusburger, J.M., et al., 2024. Expanded insights into Martian mineralogy: updated analysis of Gale crater's mineral composition via CheMin crystal chemical investigations. Minerals 14, 773.
- Peretyazhko, T., Niles, P.B., Sutter, B., Morris, R.V., Agresti, D.G., Le, L., Ming, D.W., 2018. Smectite formation in the presence of sulfuric acid: implications for acidic smectite formation on early Mars. Geochim. Cosmochim. Acta 248–260.
- Rampe, E.B., Blake, D.F., Bristow, T.F., Ming, D.W., Vaniman, D.T., Morris, R.V., Achilles, C.N., Chipera, S.J., Morrison, S.M., Tu, V.M., Yen, A.S., Castle, N., Downs, G.W., Downs, R.T., Grotzinger, J.P., Hazen, R.M., Treiman, A.H., Peretyazkho, T.S., Des Marais, D.J., Walroth, R.C., Craig, P.I., Crisp, J.A., Lafuente, B., Morookian, J.M., Sarrazin, P.C., Thorpe, M.T., Bridges, J.C., Edgar, L. A., Fedo, C.M., Freissient, C., Gellert, R., Mahaffy, P.R., Newsom, H.E., Johnson, J.R., Kah, L.C., Siebach, K.L., Schieber, J., Sun, V.Z., Vasavada, A.R., Webster, C., Wellington, D., R.C., 2020a. Wiens, and the MSL science team, mineralogy and geochemistry of sedimentary rocks and eolian sediments in Gale crater, Mars: a review after six earth years of exploration with curiosity. Geochemistry 80 (2),
- 125605. https://doi.org/10.1016/j.chemer.2020.125605.

 Rampe, E.B., Bristow, T.F., Morris, R.V., Morrison, S.M., Achilles, C.N., Ming, D.W., Vaniman, D.T., Blake, D.F., Tu, V.M., Chipera, S.J., Yen, A.S., Peretyazhko, T.S., Downs, R.T., Hazen, R.M., Treiman, A.H., Grotzinger, J.P., Castle, N., Craig, P.I., Des Marais, D.J., Thorpe, M.T., Walroth, R.C., Downs, G.W., Fraeman, A.A., Siebach, K. L., Gellert, R., Lafuente, B., McAdam, A.C., Meslin, P.-Y., Sutter, B., Salvatore, M.R., 2020b. Mineralogy of Vera Rubin ridge from the Mars science laboratory CheMin instrument. JGR: Planets 125 (9). https://doi.org/10.1029/2019JE006306.
- Rodriguez, L.E., Altair, T., Hermis, N.Y., Jia, T.Z., Roche, T.P., Steller, L.H., Weber, J.M., 2024. A Geological and Chemical Context for the Origins of Life on Early Earth, Ch 4 Astrobiology 3.0 Primer. Astrobiology 24 (S1), S-4–S-39. https://doi.org/10.1089/ ast.2021.0139.
- Rudolph, A., Horgan, B., Johnson, J., Bennett, K., Haber, J., Bell, J.F.I.I.I., et al., 2022. The distribution of clay minerals and their impact on diagenesis in Glen Torridon, Gale crater, Mars. J. Geophys. Res. 127, e2021JE007098. https://doi.org/10.1029/ 2021JE007098.
- Russell, M.J., Hall, A.J., Martin, W., 2010. Serpentinization as a source of energy at the origin of life. Geobiology 8, 5. https://doi.org/10.1111/j.1472-4669.2010.00249.x.
- Sakuma, H., Morida, K., Takahashi, Y., Fukushi, K., Noda, N., Sekine, Y., Tamura, K., 2022. Synthesis of ferrian and ferro-saponites: Implications for the structure of (Fe,

- Mg)-smectites formed under reduced conditions. Am. Mineral. 107 (10), 1926–1935. https://doi.org/10.2138/am-2022-8231.
- Schwenzer, S.P., Bridges, J.C., Wiens, R.C., Conrad, P.G., Kelley, S.P., Leveille, R., Mangold, N., Martin-Torres, J., McAdam, A., Newsom, H., Zorzano, M.P., 2016. Fluids during diagenesis and sulfate vein formation in sediments at Gale crater, Mars. Meteor. Planet. Sci. 51 (11), 2175–2202. https://doi.org/10.1111/maps 12668
- Sheppard, R.Y., Milliken, R.E., Parente, M., Itoh, Y., 2020. Updated perspectives and hypotheses on the mineralogy of lower Mt. sharp, Mars, as seen from orbit. J. Geophys. Res. 126, e2020JE006372. https://doi.org/10.1029/2020JE006372.
- Sheppard, R.Y., Thorpe, M.T., Fraeman, A.A., Fox, V.K., Milliken, R.E., 2021. Merging perspectives on secondary minerals on Mars: a review of ancient water-rock interactions in Gale crater inferred from orbital and in-situ observations. Minerals 11, 986. https://doi.org/10.3390/min11090986.
- Sherman, G.D., 1952. The titanium content of Hawaiian soils and its significance. Soil Sci. Soc. Am. J. 16, 15–18.
- Sposito, G., 1984. The Surface Chemistry of Soils. Oxford Univ Press, New York, p. 234.
 Starkey, H.C., 1982. The role of clays in fixing lithium. In: U.S. Geological Survey Bulletin, 1278-F. https://doi.org/10.3133/b1278F.
- Thomas, N.H., Ehlmann, B.L., Anderson, D.E., Clegg, S.M., Forni, O., Schröder, S., et al., 2018. Characterization of hydrogen in basaltic materials with laser-induced breakdown spectroscopy (LIBS) for application to MSL ChemCam data. J. Geophys. Res. Planets 123, 1996–2021. https://doi.org/10.1029/2017JE005467.
- Thorpe, M.T., Bristow, T.F., Rampe, E.B., Tosca, N.J., Grotzinger, J.P., Bennett, K.A., et al., 2022. Mars science laboratory CheMin data from the Glen Torridon region and the significance of lake-groundwater interactions in interpreting mineralogy and sedimentary history. J. Geophys. Res. 127, e2021JE007099. https://doi.org/10.1029/2021JE007099.
- Tu, V.M., Rampe, E.B., Bristow, T.F., Thorpe, M.T., Clark, J.V., Castle, N., Fraeman, A.A., Edgar, L.A., McAdam, A., Bedford, C., Achilles, C.N., Blake, D., Chipera, S.J., Craig, P.I., Des Marais, D.J., Downs, G.W., Downs, R.T., Fox, V., Grotzginer, J.P.,

- Hazen, R.M., Ming, D.W., Morris, R.V., Morrison, S.M., Pavri, B., Eigenbrode, J., Peretyazhko, T.S., Sarrazin, P.C., Sutter, B., Treiman, A.H., Vaniman, D.T., Vasavada, A.R., Yen, A.S., Bridges, J.C., 2021. A review of the phyllosilicates in Gale Crater as detected by the CheMin instrument on the Mars Science Laboratory, Curiosity Rover. Minerals 11 (8). https://doi.org/10.3390/min11080847.
- Vaniman, D.T., Bish, D.L., Ming, D.W., Bristow, T.F., Morris, R.V., Blake, D.F., Achilles, C.N., 2014. Mineralogy of a mudstone at Yellowknife Bay, Gale crater, Mars. Science 343 (6169), 1243480. https://doi.org/10.1126/science.1243480.
- Villumsen, A., Nielsen, O.B., 1976. The influence of paleosalinity, grain size distribution, and clay minerals on the content of B, li, and Rb in quaternary sediments of eastern Jutland, Denmark. Sedimentology 23, 845–855.
- Vine, J.D., 1980. Where is the Lithium? U.S. Geol. Surv. Bull. 1831, 31–39. https://doi. org/10.3133/b1831.
- Viviano, C.E., Moersch, J.E., McSween, H.Y., 2013. Implications for early hydrothermal environments on Mars through the spectral evidence for carbonation and chloritization reactions in the Nili Fossae region. J. Geophys. Res. Planets 118, 1858–1872. https://doi.org/10.1002/jgre.20141.
- Weber, J.M., Martinez, E.M., Sheppard, R.Y., Rodriguez, L.E., Celestian, A., Teece, B.L., Barge, L.M., 2024. Mars mineral weathering experiments in a continuous-flow reactor. Under review. Geofluids.
- Williams, L.B., Hervig, R.L., 2005. Lithium and boron isotopes in illite-smectite: the importance of crystal size. Geochim. Cosmochim. Acta 69 (22), 5705–5716. https://doi.org/10.1016/j.gca.2005.08.005.
- Wimpenny, Josh, Gíslason, Sigurður R., James, Rachael H., Gannoun, Abdelmouhcine, Pogge, Philip A.E., Strandmann, Von, Burton, Kevin W., 2010. The behaviour of Li and Mg isotopes during primary phase dissolution and secondary mineral formation in basalt. Geochim. Cosmochim. Acta 74 (18), 5259–5279. ISSN 0016–7037. htt ps://doi.org/10.1016/j.gca.2010.06.028.
- Zawidzki, M., 1976. The role of lithium in clay minerals. Geochim. Cosmochim. Acta 40 (4), 587–594. https://doi.org/10.1016/0016-7037(76)90035-7.